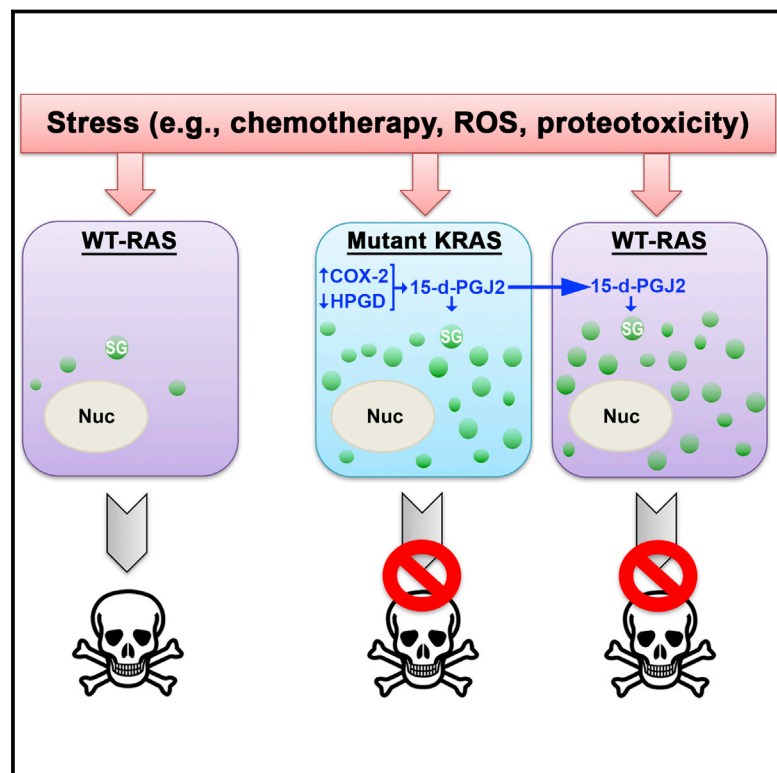


Mutant KRAS Enhances Tumor Cell Fitness by Upregulating Stress Granules

Graphical Abstract



Authors

Elda Grabocka, Dafna Bar-Sagi

Correspondence

dafna.bar-sagi@nyumc.org

In Brief

By producing a lipid molecule that promotes stress granule formation, tumor cells protect themselves and neighboring cells from the effects of stress stimuli and chemotherapy drugs.

Highlights

- Stress granules (SGs) are markedly elevated in mutant KRAS cells and tumors
- Mutant KRAS upregulates SGs by stimulating the production of 15-d-PGJ2
- 15-d-PGJ2 secretion by mutant KRAS cells enables paracrine upregulation of SGs
- Mutant KRAS-dependent upregulation of SGs confers resistance to stress stimuli



Mutant KRAS Enhances Tumor Cell Fitness by Upregulating Stress Granules

Elda Grabocka^{1,2} and Dafna Bar-Sagi^{1,3,*}

¹Department of Biochemistry and Molecular Pharmacology, New York University School of Medicine, New York, NY 10016, USA

²Present address: Department of Cancer Biology, Sidney Kimmel Cancer Center, Thomas Jefferson University, 233 South 10th Street, BLSB 1002, Philadelphia, PA 19107, USA

³Lead Contact

*Correspondence: dafna.bar-sagi@nyumc.org

<http://dx.doi.org/10.1016/j.cell.2016.11.035>

SUMMARY

There is growing evidence that stress-coping mechanisms represent tumor cell vulnerabilities that may function as therapeutically beneficial targets. Recent work has delineated an integrated stress adaptation mechanism that is characterized by the formation of cytoplasmic mRNA and protein foci, termed stress granules (SGs). Here, we demonstrate that SGs are markedly elevated in mutant KRAS cells following exposure to stress-inducing stimuli. The upregulation of SGs by mutant KRAS is dependent on the production of the signaling lipid molecule 15-deoxy- Δ 12,14 prostaglandin J2 (15-d-PGJ2) and confers cytoprotection against stress stimuli and chemotherapeutic agents. The secretion of 15-d-PGJ2 by mutant KRAS cells is sufficient to enhance SG formation and stress resistance in cancer cells that are wild-type for KRAS. Our findings identify a mutant KRAS-dependent cell non-autonomous mechanism that may afford the establishment of a stress-resistant niche that encompasses different tumor subclones. These results should inform the design of strategies to eradicate tumor cell communities.

INTRODUCTION

The acquisition of a gain-of-function mutation in the *KRAS* gene is a driver of malignant transformation in a wide number of tissues (Stephen et al., 2014). Collateral damage to the emergence of such mutations is an increase in the exposure of mutant KRAS cells to stress-inducing conditions (e.g., genotoxic, proteotoxic, and metabolic stress) due to the loss of normal proliferative barriers and the disruption of tissue homeostasis (Downward, 2015; Luo et al., 2009b). Thus, the successful expansion of KRAS tumors is dependent on the engagement of stress-adaptive mechanisms that enable cells to grow and survive under adverse conditions (Solimini et al., 2007). These stress-adaptive mechanisms are also largely responsible for the notorious drug resistance of KRAS cancers to chemotherapeutic agents (Eberhard et al., 2005; Grana et al., 2002; Rosell et al., 1995; Wang et al., 2011).

By extension, understanding the molecular mechanisms through which mutant KRAS confers stress resistance has the potential to inform the development of new targeting strategies that may have significant therapeutic implications.

Stress granules (SGs) are characterized as non-membranous cytosolic structures consisting of mRNA and protein that form upon cellular exposure to a variety of stress stimuli, including oxidative, nutritional, genotoxic, proteotoxic, and osmotic stress, UV irradiation and chemotherapeutic agents and are required for cells to cope with stress (Kedersha et al., 2013). The current view holds that SG assembly occurs downstream of stress-induced translational arrest, with the pool of stalled mRNAs serving as the scaffold for the recruitment of RNA-binding proteins, which, in turn, recruit a plethora of signaling molecules (Anderson et al., 2015; Buchan and Parker, 2009; Kedersha et al., 2013). As such, SGs are thought to operate as platforms for signal compartmentalization and regulation of pathway activity. In support of this idea, the recruitment of TORC1 and dual specificity tyrosine phosphorylation-regulated kinase (DYRK) 3 to SGs has been shown to regulate the timing of TORC1 inactivation and reactivation in stressed cells (Wippich et al., 2013). In addition, it has been demonstrated that the association of RACK1 with SGs leads to the inhibition of stress-induced activation of p38/JNK signaling, thereby compromising p38/JNK-mediated apoptosis (Arimoto et al., 2008).

While the critical role of SGs in the cellular stress response is well established, their contribution to tumor cell fitness is less understood. Here, we demonstrate that SG formation is elevated in mutant KRAS cells in response to a variety of stress stimuli. The upregulation of SGs is mediated by mutant KRAS-dependent pathways that control prostaglandin metabolism and confer cytoprotection by cell autonomous and cell non-autonomous mechanisms. Intercepting these pathways leads to the sensitization of mutant KRAS cells to stress stimuli and chemotherapeutic agents. Our results define a previously unappreciated paracrine mechanism exploited by mutant KRAS tumors to counteract stress. This mechanism could serve to establish a stress-resistant environment consisting of cells with diverse genetic and lineage backgrounds, and, as such, may dictate responsiveness to therapeutic intervention.

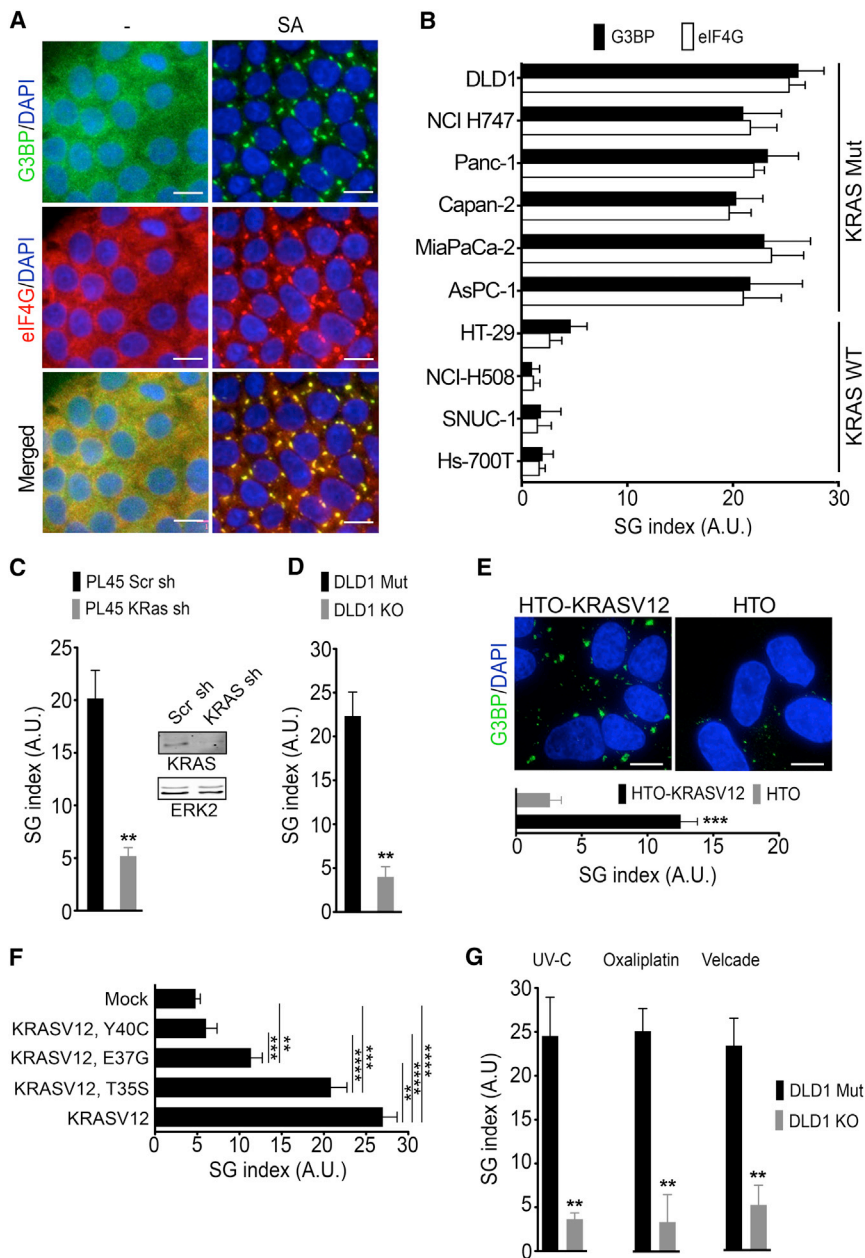


Figure 1. Upregulation of SGs in Mutant KRAS Cells

(A) DLD1 Mut cells were treated with sodium arsenate (SA, 100 μ M) for 1 hr. SGs were detected by G3BP and eIF4G immunofluorescence staining. Scale bars, 10 μ m.

(B) Colon (DLD1, NCI H747, HT29, NCI H508, SNUC1) and pancreatic (Panc-1, Capan-2, MiaPaCa 2, AsPC-1, HS 700T) cancer cells were treated as in (A). SGs were quantified by defining a SG index (SG area/cell area) based on G3BP and eIF4G immunofluorescence. Data are presented as arbitrary units (a.u.). Error bars indicate mean \pm SEM for at least three independent experiments in which four fields of view with at least 50 cells per field of view per cell line were quantified.

(C) PL45 cells expressing inducible scramble (Scr) or KRAS shRNA were treated with SA as in (A). The SG index based on G3BP immunofluorescence is shown. (Inset) Whole cell lysates (WCL) expressing inducible scramble (Scr) or KRAS shRNA were subjected to immunoblotting with the indicated antibodies. ERK2 serves as a loading control.

(D) DLD1 Mut and DLD1 KO cells were treated with SA as in (A). The SG index based on G3BP immunofluorescence is shown.

(E) HeLa Tet-ON cells (HTO) and HTO cells that conditionally express mutant KRAS (HTO-KRASV12) were treated with SA (100 μ M, 1 hr). SGs were visualized by G3BP immunofluorescence staining (top). The SG index based on G3BP immunofluorescence is shown (bottom). Scale bars, 10 μ m.

(F) HeLa cells expressing mCherry-KRASV12, mCherry-KRASV12T35S, mCherry-KRASV12E37G, and mCherry-KRASV12Y40C were treated with SA (100 μ M, 1 hr). The SG index based on G3BP immunofluorescence is shown.

(G) DLD1 Mut and DLD1 KO cells were treated with UV-C irradiation (50 mJ/m², 24 hr), oxaliplatin (200 μ M, 6 hr), or velcade (1 μ M, 8 hr). The SG index based on G3BP immunofluorescence is shown.

(C–G) Data are from a representative experiment out of at least three independent experiments. For all graphs, error bars indicate mean \pm SEM for at least four fields of view with at least 50 cells per field of view. ***p* < 0.05, ****p* < 0.005, *****p* < 0.005. See also Figure S1.

RESULTS

SG Formation in Response to Stress Exposure Is Upregulated in Mutant KRAS Cells

To monitor SG formation, we have used a well-documented assay in which the cellular distribution of SG resident proteins is assessed by immunofluorescence (Kedersha and Anderson, 2007). As illustrated in Figure 1A, exposure of mutant KRAS colorectal cancer cells DLD1 (hereafter referred to as DLD1 Mut) to oxidative stress via treatment with sodium arsenate (SA) was associated with the induction of SGs as indicated by the accumulation of cytoplasmic puncta containing two well-established SG markers: endogenous endoribonuclease RAS GTPase-acti-

vating protein-binding protein 1 (G3BP) and endogenous eukaryotic initiation factor 4G (eIF4G) (Kedersha and Anderson, 2007). To establish a quantitative readout for SG formation, we applied the ImageJ analyze-particle tool to calculate the fraction of the total area of SGs in the total cell area visualized. Using this approach, we compared the induction of SGs in response to oxidative stress across a panel of human pancreatic and colorectal adenocarcinoma cell lines (Figure 1B). This analysis revealed that the levels of SGs displayed by mutant KRAS negative (KRAS wild-type [WT]) cancer cells, including cancer cells that harbored oncogenic mutations in BRAF (HT-29) or BRAF/PI3K (NCI H747), was significantly lower compared to cancer cells that harbored KRAS mutations (KRAS Mut). Together, these

observations suggest that mutant KRAS may play a regulatory role in SG formation.

Mutant KRAS Is Necessary and Sufficient for SG Upregulation

To determine whether mutant KRAS is a causative factor leading to elevated SG levels, we assessed SG formation under experimental conditions where mutant KRAS expression was conditionally suppressed or switched on. Inducible short hairpin RNA (shRNA)-directed knockdown of KRAS in the KRAS mutant pancreatic cancer cell lines PL45, Panc-1, MiaPaCa-2, and AsPC-1 resulted in a significant attenuation of SG formation in response to oxidative stress (Figures 1C and S1A). In addition, SG formation was reduced by approximately 5-fold in an isogenic derivative of DLD1 Mut cells where the mutant *KRAS* allele had been knocked out (DLD1 knockout [KO]) (Shirasawa et al., 1993), (Figures 1D and S1B). Conversely, inducible expression of mutant KRAS (KRASV12) in HeLa Tet-ON KRASV12 cells led to an approximate 5-fold elevation in SG levels following exposure to oxidative stress (Figure 1E). Upregulation of SGs by mutant KRAS was reflected in significantly larger average size and number of SGs per cell (Figure S1C). Together, these observations indicate that mutant KRAS is necessary and sufficient for SG upregulation under oxidative stress conditions. Moreover, expression of mutant HRAS (HRASV12) also enhanced SG levels, indicating that acquisition of an activating mutation in other RAS isoforms also confers SG upregulation (data not shown).

To define the molecular pathways through which mutant KRAS upregulates SGs, we investigated three key Ras-effector pathways: KRAS/RAF, KRAS/RALGEF, and KRAS/PI3K. To do so, we utilized the RAS effector domain mutants KRASV12,T35S, KRASV12,E37G, or KRASV12,Y40C, which preferentially activate the RAF, RALGEF, or PI3K pathway, respectively. HeLa cells transiently expressing KRASV12,T35S upregulated SGs ~5-fold over mock transfected cells, similar to KRASV12-expressing cells (Figure 1F). In contrast, HeLa cells expressing KRASV12,Y40C showed no upregulation, whereas expression of KRAS,V12E37G led to a modest upregulation (~2-fold) (Figure 1F). These results implicate the RAF pathway as a major mediator for KRAS-induced SG upregulation. Consistent with this, treatment with the MEK inhibitor PD0325901 impaired the capacity of HeLa Tet-ON KRASV12 cells to form SGs (Figure S1D).

In addition to oxidative stress, several other tumor-associated stresses have been shown to induce SGs (Arimoto et al., 2008; Dewey et al., 2011; Kedersha and Anderson, 2007; Moeller et al., 2004). To test whether mutant KRAS-dependent upregulation of SGs displays specificity for a particular type of stress, we subjected DLD1 Mut and DLD1 KO cells to various stress stimuli. As illustrated in Figure 1G, the presence of mutant KRAS was associated with elevated levels of SG induction in response to ultraviolet C (UV-C) irradiation (~6-fold) and the chemotherapeutic agents oxaliplatin (~6-fold) and velcade (~5-fold), which induce DNA damage and proteotoxic stress, respectively. These results are consistent with a role for mutant KRAS in regulating fundamental aspects of SG formation that are common to diverse stress stimuli.

SGs are dynamic structures that form and dissipate with kinetics that can vary depending on the type of stress (Kedersha

and Anderson, 2007; Kedersha et al., 2008). Time-course analysis of SG levels revealed that DLD1 Mut cells displayed more than 5-fold elevation of SG levels relative to DLD1 KO cells at the 30 min time point following exposure to sodium arsenate, and this trend was maintained until their dissolution at the 120 min time point (Figure S1E). Similarly, DLD1 Mut cells showed ~5-fold elevated SG levels compared to DLD1 KO cells at 3 hr following UV-C irradiation, when SGs start to become apparent, and a similar trend is maintained for the 24 hr time course after which SGs dissipate (Figure S1F and data not shown). Similar results were obtained for oxaliplatin and velcade (data not shown). Together, these results indicate that mutant KRAS promotes the rate and extent of SG formation.

Mutant KRAS Tumors Display Elevated Levels of SGs

To investigate whether the effect of mutant KRAS on SG levels observed in cell culture conditions is manifested in vivo, we evaluated SGs in the pancreata of *LSL-KRasG12D/+;LSL-Trp53R172H/+;Pdx-1-Cre (KPC)* mice (Hingorani et al., 2005). As shown in Figure 2A, the SG marker G3BP showed a diffuse cytoplasmic distribution in normal pancreatic tissue. In contrast, G3BP accumulated in cytoplasmic granular structures in the majority of lesions resembling early pancreatic intraepithelial neoplasia (PanINs) and in all lesions displaying a phenotype of advanced PanINs. Importantly, SGs were readily detected in tissue sections from human pancreatic adenocarcinoma, as visualized by G3BP (Figure 2B) or poly A mRNA binding protein 1 (PABP1) (Figure S2A) staining, but not in adjacent normal pancreatic tissue (Figure 2C). Furthermore, SGs were prominent in human xenograft tumors from the KRAS mutant cell lines DLD1 Mut and PL45 (Figure S2B). In comparison, no SGs were detected in xenografts of the KRAS WT cell line BxPC3 (Figure S2B), affirming that the upregulation of SGs in vivo is associated with the presence of mutant KRAS.

Mutant KRAS-Induced Upregulation of SGs Is Mediated by eIF4A

We next sought to determine the mechanism through which mutant KRAS promotes SG upregulation. The main regulatory events that have been identified as essential for SG formation are the phosphorylation of the eukaryotic initiation factor eIF2 α and the inactivation of the eukaryotic initiation factor eIF4A (Kedersha et al., 2013). Both events lead to a decrease in translation initiation rates, which provides the surge in non-polysomal RNA, which functions as a scaffold for SG nucleator proteins. In addition, overexpression of SG nucleating proteins can lead to SG assembly, even in the absence of stress stimuli (Kedersha and Anderson, 2007). We first asked whether upregulated SG levels in DLD1 Mut versus DLD1 KO cells occur as a consequence of increased eIF2 α phosphorylation. Both DLD1 Mut and DLD1 KO cells displayed similar levels of p-eIF2 α following exposure to sodium arsenate or oxaliplatin, demonstrating that elevated SG levels in DLD1 Mut cells cannot be merely attributed to higher p-eIF2 α levels (Figure 3A and data not shown). Of note, neither sodium arsenate nor oxaliplatin treatment led to an increase in the phosphorylation of eIF2 α over basal levels (Figure 3A and data not shown), consistent with earlier reports demonstrating that eIF2 α is constitutively

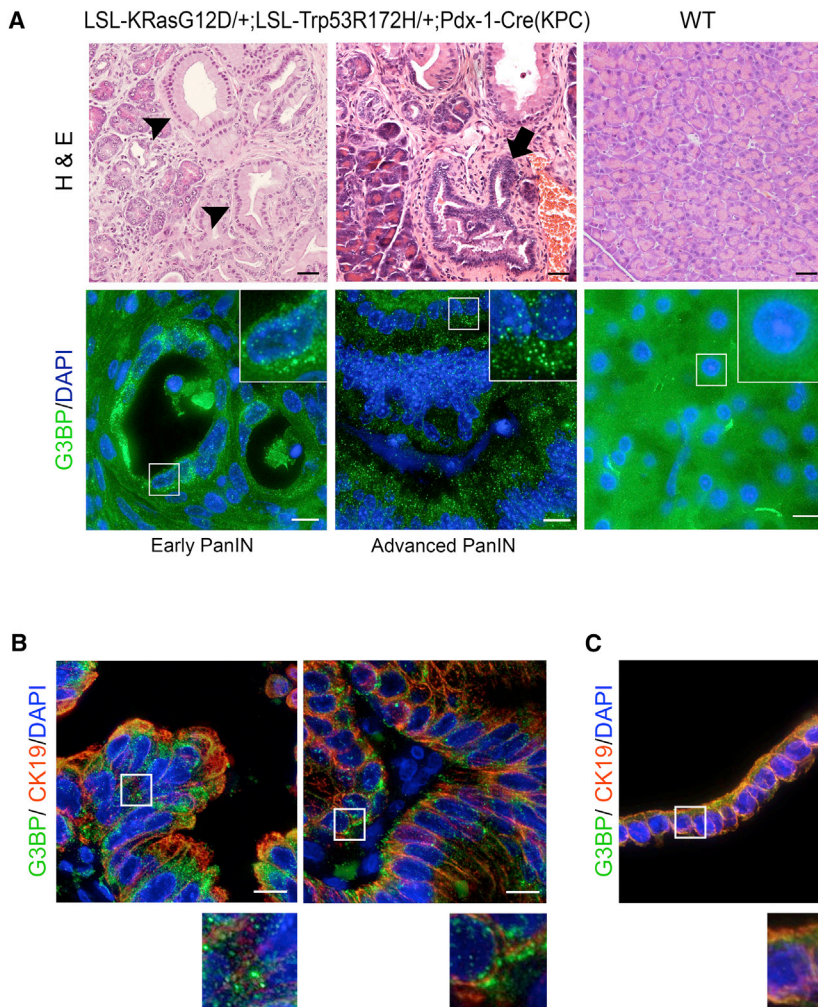


Figure 2. Mutant KRAS Upregulates SGs In Vivo

(A) Serial sections from pancreata of *LSL-KRasG12D/+;LSL-Trp53R172H/+;Pdx-1-Cre* (KPC) animals and control wild-type (WT) littermates were stained with H&E (scale bar, 40 μ m), and SGs were visualized by G3BP immunofluorescence (scale bar, 10 μ m; inset, 4 \times zoom-in of boxed region). Arrowheads and arrows indicate early and advanced PanIN lesions, respectively. Images are representative of results obtained from three animals per cohort.

(B) Sections from two independent human PDAC tissues were immunostained for G3BP and CK19 (epithelial marker).

(C) A section from a normal region in human PDAC immunostained for G3BP and CK19.

(B and C) Scale bar, 10 μ m. Lower panels are 3 \times zoom-in of boxed regions.

See also Figure S2.

phosphorylated in cancer cells (Silvera et al., 2010). Furthermore, DLD1 Mut and DLD1 KO cells showed similar levels of G3BP and eIF4A (Figure 3A), ruling out the possible contribution of a preferential increase in the levels of these SG nucleators.

We next examined whether mutant KRAS regulates SGs through eIF4A inactivation. A characteristic property of eIF4A-regulated SGs is the presence of eIF2 α and eIF5 initiation factors, which are absent from p-eIF2 α -dependent SGs (Bordeleau et al., 2005; Silvera et al., 2010). Consistent with mutant KRAS-driven SG upregulation being dependent on eIF4A inactivation, but not eIF2 α phosphorylation, SGs in the KRAS mutant cells DLD1 Mut and MiaPaCa2 were positive for eIF2 α and eIF5 (Figures 3B and S3A). The inactivation of eIF4A and the consequential induction of SGs has been reported to occur through covalent modification of eIF4A by the bioactive lipid prostaglandins 15-deoxy-delta 12,14-prostaglandin J2 (15-d-PGJ2) and prostaglandin A1 (PGA1) (Kim et al., 2007). We reasoned that if SG upregulation by mutant KRAS is mediated by 15-d-PGJ2-dependent inactivation of eIF4A, then the treatment of cells with 15-d-PGJ2 would obviate the requirement of mutant KRAS for the upregulation of SGs. Consistent with this postulate, incuba-

tion of DLD1 KO cells with 15-d-PGJ2 was sufficient to induce the accumulation of SGs to a similar level to that was observed in DLD1 Mut cells (Figures 3C and S3B). This effect was specific to 15-d-PGJ2, because the addition of another prostaglandin, prostaglandin E2 (PGE2), did not induce SGs (Figure S3C).

Mutant KRAS Enhances SG Formation by Regulating Prostaglandin Biosynthesis and Catabolism

The capacity of 15-d-PGJ2 to enhance SG formation raises the possibility that, in mutant KRAS cells, this response might

be linked to mutant KRAS-regulated changes in prostaglandin levels. The accumulation of prostaglandin in tissues is controlled by the relative rates of biosynthesis and breakdown. The rate-limiting step in prostaglandin biosynthesis is catalyzed by cyclooxygenases (COX) 1 and/or 2, whereas prostaglandin degradation is catalyzed by the NAD⁺-dependent 15-hydroxyprostaglandin dehydrogenase (HPGD). Suppression of mutant KRAS expression in colon and pancreatic cancer cells led to an attenuation of *PTGS2* (COX-2) levels and an upregulation of HPGD (Figures 3D, 3E, and S3D). These results suggest that mutant KRAS can control prostaglandin accumulation by enhancing biosynthesis and/or attenuating catabolism. In support of this idea, analysis of ONCOMINE data from tissue samples from pancreatic adenocarcinomas where KRAS mutations are highly prevalent (~90% of patients) revealed significant *PTGS2* upregulation as well as *HPGD* downregulation compared to normal pancreatic tissue (Figure S3E). Consistent with a regulatory role for mutant KRAS in prostaglandin accumulation, we also observed a significant enrichment of *PTGS2* in lung adenocarcinoma (LUAD) tumors with KRAS mutations compared to tumors with wild-type KRAS (Figure S3F).

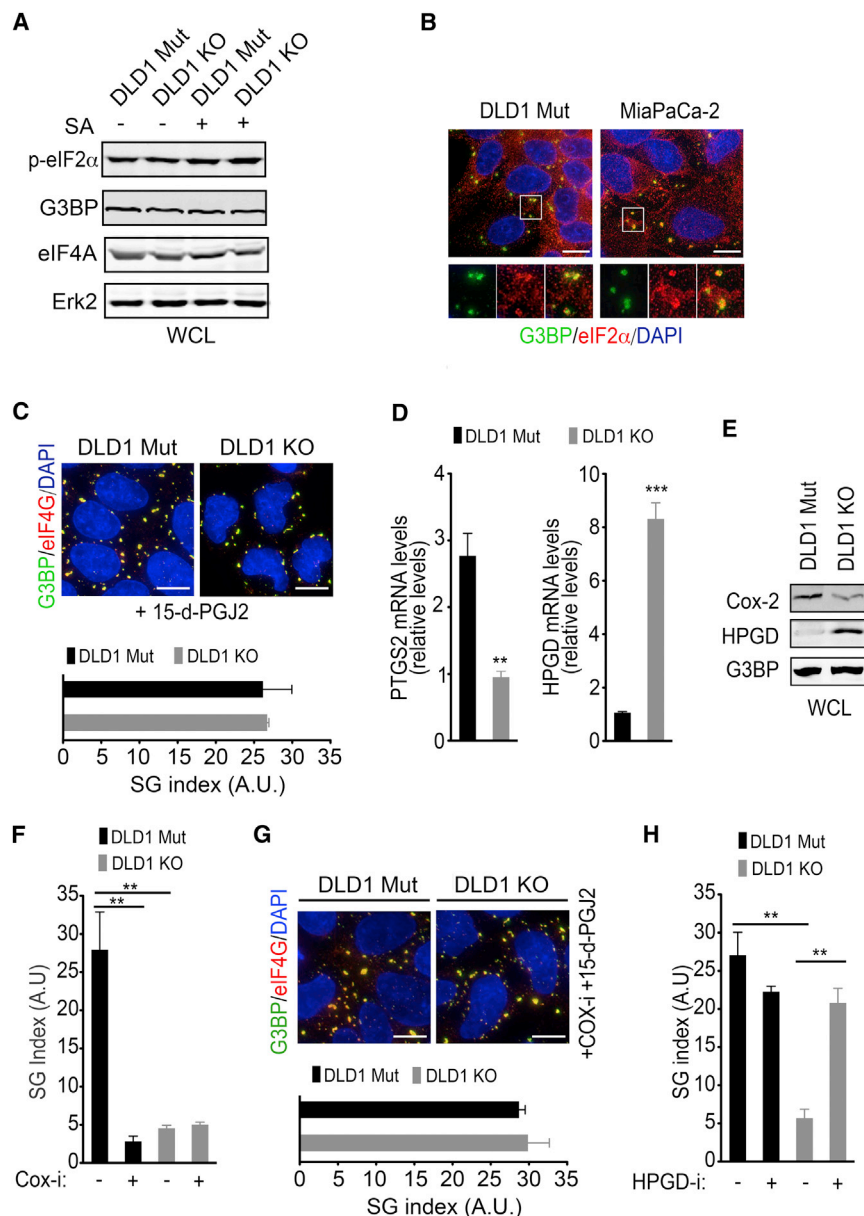


Figure 3. Mutant KRAS Upregulates SGs by Modulating the Cellular Capacity to Biosynthesize and Catabolize Prostaglandins

(A) DLD1 Mut and DLD1 KO cells were treated with SA (100 μ M, 1 hr). Whole cell lysates (WCL) were collected and subjected to immunoblotting with the indicated antibodies. ERK2 serves as a loading control.

(B) DLD1 Mut and MiaPaCa-2 cells were treated with SA as in (A), and SGs were detected by immunofluorescence staining for G3BP and eIF2 α . (C) DLD1 Mut and DLD1 KO cells were treated with 15-d-PGJ2 (50 μ M, 1 hr). SGs were detected by immunofluorescence staining for G3BP and eIF4G (top). The SG index based on G3BP immunofluorescence (bottom) is shown.

(D) PTGS2 and HPGD mRNA levels in DLD1 Mut and DLD1 KO cells were assessed by qRT-PCR. Error bars indicate SEM (n = 3).

(E) COX-2 and HPGD protein levels in DLD1 Mut and DLD1 KO cells were assessed by immunoblotting of whole cell lysates (WCL) with the indicated antibodies. G3BP serves as a loading control.

(F) DLD1 Mut cells were treated with diclofenac sodium (20 μ M, COX-i) for 12 hr followed by SA treatment (100 μ M, 1 hr). The SG index based on G3BP immunofluorescence is shown.

(G) DLD1 Mut and DLD1 KO cells were treated with diclofenac sodium (COX-i) as in (F) and 15-d-PGJ2 as in (C). SGs were detected by immunofluorescence staining for G3BP and eIF4G (top). The SG index based on G3BP immunofluorescence is shown (bottom).

(H) DLD1 Mut and DLD1 KO cells were treated with an HPGD inhibitor (HPGD-i; 40 μ M) for 6 hr followed by SA (100 μ M, 1 hr). The SG index based on G3BP immunofluorescence is shown.

(A–C and E–H) Data are from a representative experiment out of at least three independent experiments.

(C and F–H) Error bars indicate mean \pm SEM for at least four fields of view with at least 50 cells per field of view.

p < 0.005, *p < 0.0005. Scale bars, 10 μ m. See also Figure S3.

To investigate the significance of mutant KRAS-mediated prostaglandin accumulation in SG upregulation, we used pharmacological inhibitors of the relevant enzymatic activities. COX-1/2 inhibition attenuated SG levels in DLD1 Mut cells subjected to sodium arsenate (Figures 3F and S3G), and this effect was reversed by the addition of 15-d-PGJ2 (Figure 3G). Furthermore, in DLD1 KO cells, pharmacological inhibition of HPGD rescued the levels of oxidative stress-induced SGs (Figures 3H and S3H). Taken together, these results indicate that the increase in prostaglandin levels by upregulating prostaglandin biosynthesis and/or downregulating prostaglandin catabolism is essential for mutant KRAS-induced upregulation of SGs.

Mutant KRAS Exerts Cell Non-autonomous Control of SG Levels through 15-d-PGJ2

Because 15-d-PGJ2 is a secreted molecule, in principle, it could regulate its targets in a cell autonomous and/or cell non-autonomous fashion. This raises the possibility that, by regulating 15-d-PGJ2 production, mutant KRAS might exert cell non-autonomous control of SG levels. To test this idea, we initially measured the extracellular amounts of 15-d-PGJ2 and its precursor PGD2 by ELISA. The levels of 15-d-PGJ2 and PGD2 detected in conditioned medium from DLD1 Mut cells (KRAS conditioned medium [KCM]) were significantly higher compared with DLD1 KO cells (Figure 4A). Furthermore, conditioned media from MiaPaCa-2 and AsPC-1 cells, in which KRAS has been knocked down, had

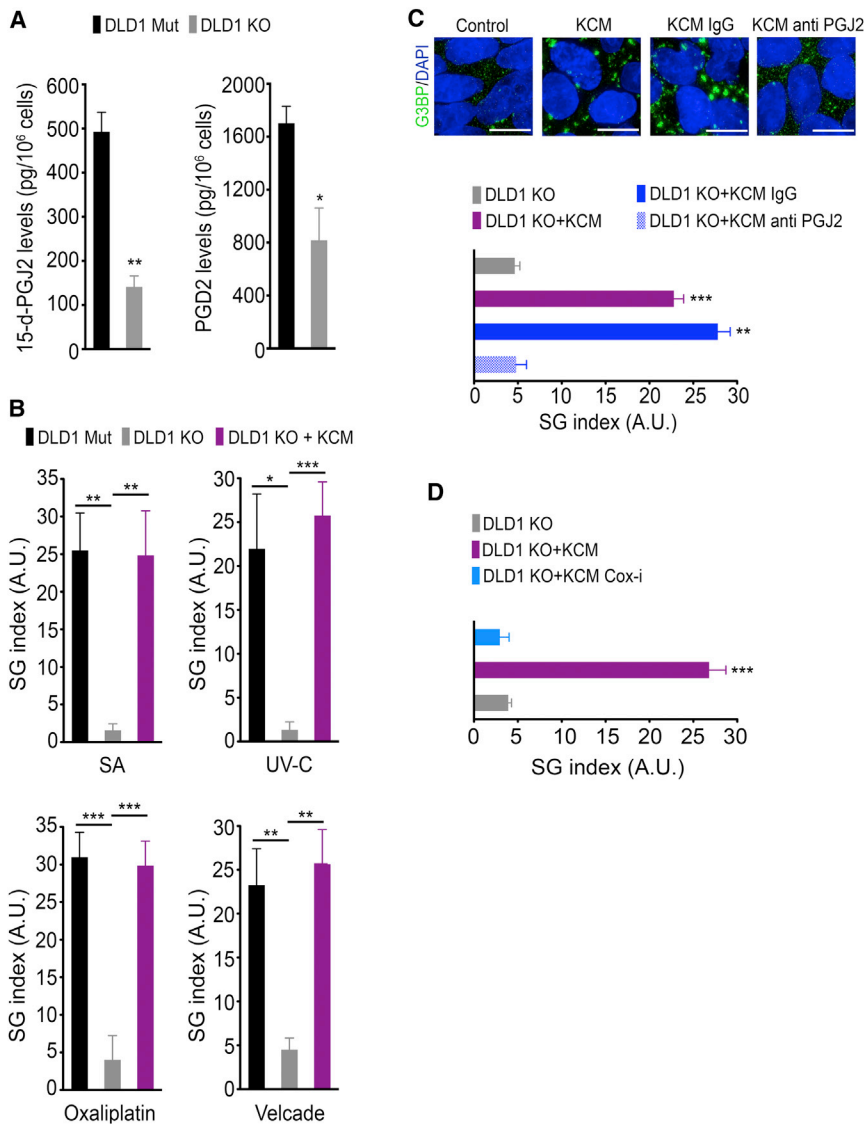


Figure 4. Cell Non-autonomous Upregulation of SGs by Mutant KRAS Is Mediated by 15-d-PGJ2

(A) The levels of 15-d-PGJ2 and PGD2 that were secreted by DLD1 Mut and DLD1 KO cells were determined by ELISA of the respective cell culture medium. Data are represented as mean \pm SEM. (B) DLD1 Mut and DLD1 KO cells were incubated for 10 min in control medium or in conditioned medium from DLD1 Mut cells (KRAS-conditioned media [KCM]) and then treated with SA, UV-C irradiation, oxaliplatin, or velcade as in Figure 1G. The SG index based on G3BP immunofluorescence is shown. (C) DLD1 KO cells were incubated as in (B) in control medium, KCM, KCM immunodepleted with anti-IgG (KCM IgG), or KCM immunodepleted with anti-15-d-PGJ2 (KCM anti PGJ2) and then treated with SA (100 μ M, 1 hr). SGs were detected by G3BP immunofluorescence staining (top). The SG index based on G3BP immunofluorescence is shown (bottom).

(D) DLD1 KO cells were incubated as in (B) in control medium, KCM, or KCM from cells treated with diclofenac sodium (COX-i) and then treated with SA (100 μ M, 1 hr). The SG index based on G3BP immunofluorescence is shown. Data are from a representative experiment out of at least three independent experiments. Error bars indicate mean \pm SEM for at least four fields of view. * $p < 0.05$, ** $p < 0.005$, *** $p < 0.0005$. Scale bars, 10 μ m.

See also Figure S4.

Moreover, KCM from DLD1 Mut cells that had been treated with a COX-1/2 inhibitor failed to exhibit the stimulatory effect on SG formation in DLD1 KO cells (Figure 4D), supporting a role for prostaglandin biosynthesis in the cell non-autonomous regulation of SGs. Altogether, these results establish 15-d-PGJ2 as a secreted molecule through which

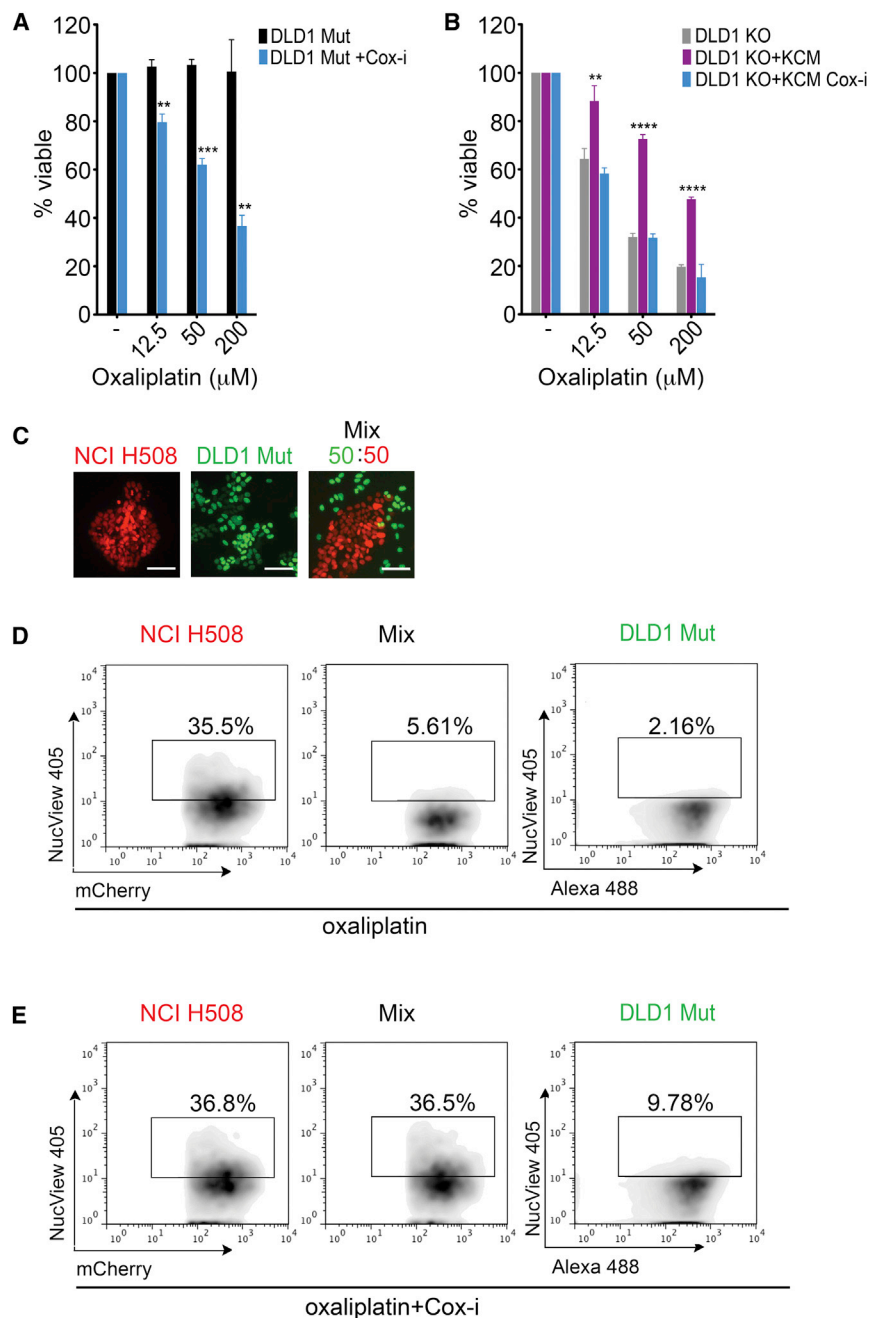
significantly lower levels of 15-d-PGJ2 compared to MiaPaCa-2 and AsPC-1 shRNA control cells (Figure S4). These results demonstrate that mutant KRAS promotes the extracellular accumulation of 15-d-PGJ2.

Next, we investigated the effects of KCM on SG levels in KRAS WT cells. Incubation of DLD1 KO in KCM from DLD1 Mut cells resulted in SG upregulation in response to oxidative stress, UV-C irradiation, oxaliplatin-induced DNA damage, and velcade-induced proteotoxic stress (Figure 4B). KCM from DLD1 Mut cells also led to a significant enhancement of SG levels in RAS WT 5637 bladder cancer cells and HeLa cells, confirming that this is not a cell-type-specific effect (data not shown). To formally prove that 15-d-PGJ2 is directly responsible for the SG-enhancing activity displayed by KCM, we performed an immunodepletion experiment using a 15-d-PGJ2 antibody. The capacity of KCM from DLD1 Mut cells to upregulate SGs in DLD1 KO cells was abolished following 15-d-PGJ2 immunodepletion (Figure 4C).

mutant KRAS cells modulate SG levels in a cell non-autonomous fashion.

Cell Non-autonomous Upregulation of SGs by Mutant KRAS Confers Cytoprotection from Stress Stimuli

Because SGs have been shown to be critical for cellular survival in response to stress, we asked whether SGs could contribute to mutant KRAS-mediated resistance to stress stimuli and chemotherapeutic agents. Inhibition of SGs by emetine treatment, which stalls mRNA in polysomes and thus blocks SG assembly, enhanced oxidative stress-induced apoptosis in mutant KRAS-expressing HTO-KRASV12, but not in HTO wild-type cells (Figures S5A and S5B). In addition, treatment of DLD1 Mut cells with a COX-1/2 inhibitor, which inhibits SG formation, enhanced sensitivity to oxaliplatin (Figure 5A). Taken together, these results indicate a dependence of mutant KRAS cells on SGs for resistance to stress stimuli.



We next tested whether the cell non-autonomous upregulation of SGs could also confer cytoprotection against stress stimuli. To do so, DLD1 KO cells were incubated with normal growth medium, KCM from DLD1 Mut cells, or KCM from COX-1/2 inhibitor-treated DLD1 Mut cells in the presence or absence of oxaliplatin (Figure 5B). KCM from DLD1 Mut cells reduced the sensitivity of DLD1 KO cells to oxaliplatin treatment, and this protective effect was lost when the KCM was derived from COX-1/2-inhibited DLD1 Mut cells (Figure 5B). Thus, COX-1/2-mediated cell non-autonomous upregulation of SGs might serve as a mechanism by which mutant KRAS

cells can impart resistance to chemotherapeutic agents for KRAS WT cells. Next, we asked whether this mode of cytoprotection could also occur under conditions that mimic the mutational heterogeneity observed in KRAS-driven tumors. Patient biopsies have identified tumors where mutant KRAS cancer cells co-exist with mutant PI3K cancer cells or where mutant RAS clones arise after treatment of BRAF mutant tumors with BRAF inhibitors (Baldus et al., 2010; Kopetz et al., 2015; Nazarian et al., 2010; Poulidakos et al., 2011; Richman et al., 2011). Accordingly, we co-cultured DLD1 Mut and NCI-H508 (BRAF mut/PI3K mut) cells that stably express GFP-H2B and mCherry-H2B, respectively (Figure 5C). This differential labeling of the cells allowed us to quantify the level of cell death in each cell type after treatment with oxaliplatin by flow cytometry using the NucView 405-Caspase 3 reporter (Figures 5D and 5E). Oxaliplatin had little effect on the viability of DLD1 Mut cells, whereas it induced appreciably higher levels of cell death in NCI-H508 cells (Figure 5D). However, when co-cultured with DLD1 Mut

Figure 5. KRAS Cancer Cells Exert Cell Non-autonomous Protection from Chemotherapeutic Agents via SG Upregulation

(A) Medium obtained from DLD1 Mut cells treated with or without diclofenac sodium (COX-i) was utilized to dilute oxaliplatin at the indicated concentrations and added back to the respective conditions for 48 hr. Cell viability was assessed using the 3-(4,5-dimethylthiazol-2-yl)-2,5-diphenyltetrazolium bromide (MTT) assay.

(B) Medium from DLD1 KO cells (control medium), KCM, and KCM from diclofenac sodium (COX-i)-treated cells was used to dilute oxaliplatin to the indicated concentrations and added to DLD1 KO cells. Cell viability was assessed using the MTT assay after 48 hr.

(C) Fluorescence images of mCherry-H2B-labeled NCI H508 cells (red) and GFP-H2B-labeled DLD1 Mut cells (green), cultured individually or as a mixture. Scale bars represent 40 μm.

(D) The indicated cells lines were labeled and cultured as in (C) and subjected to oxaliplatin (100 μM, 48 hr). Cell death in each population was assessed by flow cytometry analysis of NucView Alexa 405-positive cells.

(E) The indicated cells lines were cultured as in (C) and subjected to diclofenac sodium (20 μM, COX-i) as in Figure 4D, followed by oxaliplatin (100 μM) for 48 hr. Cell death in each population was assessed as in (D).

(A and B) Data are expressed as a percentage of viable cells. Error bars are mean ± SEM from three independent conditions, each performed in triplicate. **p < 0.05, ***p < 0.005, ****p < 0.0005.

(D and E) Data are from a representative experiment out of at least three independent experiments.

See also Figure S5.

cells can impart resistance to chemotherapeutic agents for KRAS WT cells.

Next, we asked whether this mode of cytoprotection could also occur under conditions that mimic the mutational heterogeneity observed in KRAS-driven tumors. Patient biopsies have identified tumors where mutant KRAS cancer cells co-exist with mutant PI3K cancer cells or where mutant RAS clones arise after treatment of BRAF mutant tumors

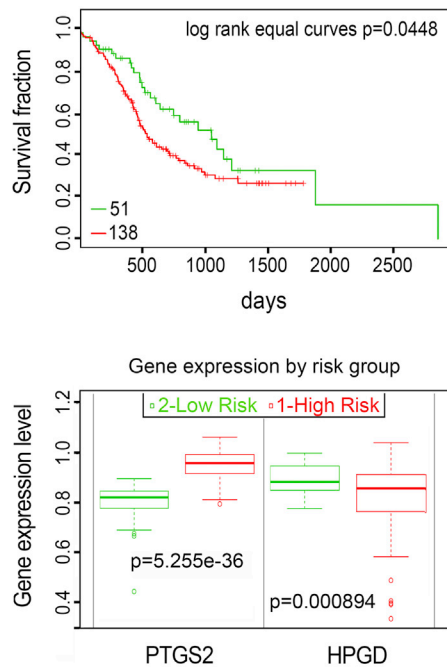


Figure 6. Expression Levels of Regulators of SGs Correlate with Poor Survival in Human Pancreatic Cancers

Kaplan-Meier survival curves of censored COX analysis showing overall survival for PACA-AU-ICGC human pancreatic carcinoma cohort (top) stratified by maximized *PTGS2* and *HPGD* expression risk groups for the respective cohorts (bottom) (SurvExpress). Error bars indicate SD. See also Figure S6.

cells, NCI-H508 displayed a markedly reduced sensitivity to oxaliplatin (Figure 5D). Notably, this reduced sensitivity to oxaliplatin correlated with significantly higher levels of SGs (~13-fold increase) in NCI-H508 cells when co-cultured with DLD1 Mut cells, compared to when cultured alone (Figures S5C and S5D). Consistent with mutant KRAS cells conferring cell non-autonomous drug resistance via the upregulation of SGs, treatment of the co-cultures with a COX1/2 inhibitor impaired the ability of DLD1 Mut cells to confer cytoprotection (Figure 5E).

Positive Regulators of SGs in Patients of Pancreatic Adenocarcinoma Are Linked to Poor Survival

Our results indicate that cell non-autonomous upregulation of SGs by mutant KRAS may affect the stress resistance properties of the tumor ecosystem. As such, the status of SG regulators and the presence of SGs in human tumors could serve as predictors of tumor fitness and drug resistance. To investigate this idea, we examined the relationship between patient survival and the levels of SG regulators identified by our study: *PTGS2* (COX-2) and *HPGD*. Kaplan-Meier curves of a human pancreatic carcinoma cohort stratified by maximized *PTGS2* and *HPGD* expression risk groups revealed that a significant subgroup (~70% of patients) with anticipated high levels of SGs (high COX-2; low HPGD) had lower overall survival (Figure 6). Because ~90% of pancreatic adenocarcinomas manifest KRAS mutations, this stratification of survival based on anticipated SG levels would suggest that SG upregulation may represent an important

mechanism through which mutant KRAS may confer tumor fitness and reduced survival. In support of this idea, we found that high *PTGS2* expression was significantly associated with poorer recurrence-free survival (RFS) in TCGA colon adenocarcinoma (COAD) patients with KRAS-mutated tumors (Figure S6). Conversely, in the absence of KRAS mutations, high *PTGS2* levels showed no significant effect on patient RFS. These observations suggest that SG upregulation may have important implications for the fitness of mutant KRAS tumors. Clearly, additional in vivo studies will be required to determine the role of SGs in tumor drug response and whether SG levels and *PTGS2*/*HPGD* expression are prognostic or predictive of tumor progression and therapy response.

DISCUSSION

The tumorigenic process subjects cancer cells to a variety of stresses that function as selection barriers and force the emergence of cells that are resistant to the adverse effects of stress. Increasing evidence indicates that the acquisition of stress resistance mechanisms by cancer cells not only provides them with a survival advantage, but is also associated with a diminished sensitivity to standard-of-care cytotoxic chemotherapies and targeted therapies (Pazarentzos and Bivona, 2015; Solimini et al., 2007). In this study, we have identified a mutant KRAS-dependent capability of cancer cells to self-protect against stress-inducing stimuli and chemotherapeutic agents through the upregulation of SGs. Furthermore, we show that this protective mechanism can be engaged in both a cell autonomous and cell non-autonomous fashion, thereby enabling the stress adaptation of tumor cell communities.

Mutant KRAS-driven cancers are extremely refractory to standard chemotherapeutic treatments (McCormick, 2015). Efforts to understand the molecular mechanisms underlying the therapeutic resistance of KRAS tumors have largely focused on RAS-regulated events that impinge on drug delivery and cell survival (Chin et al., 1992; Zuber et al., 2000; Faber et al., 2014; Hata et al., 2014). Recent studies have indicated that SGs can limit the efficacy of several chemotherapeutic agents, such as platinum compounds, 5 fluorouracil (5-FU), bortezomib, and the multikinase inhibitor sorafenib (Adjibade et al., 2015; Fournier et al., 2010; Kaehler et al., 2014). Our results demonstrate that mutant KRAS is sufficient and necessary for the upregulation of SGs in response to stress stimuli and chemotherapeutic agents (Figure 1). When the capacity of mutant KRAS is abrogated, the sensitivity of mutant KRAS cells to the chemotherapeutic agent oxaliplatin is greatly enhanced (Figures 4 and 5). Altogether, these findings suggest that therapies aimed at inhibiting SGs may provide a potential avenue to enhance the efficacy of chemotherapeutic agents in mutant KRAS cancers.

Our results identify 15-d-PGJ2 as a critical mediator of mutant KRAS-dependent SG upregulation. We propose that mutant KRAS drives the production of this prostaglandin metabolite by regulating two critical steps in prostaglandin metabolism: COX-2-mediated prostaglandin biosynthesis and HPGD-mediated prostaglandin catabolism. This postulate is based on our findings that mutant KRAS promotes the expression of COX-2

and suppresses the expression of HPGD. While the induction of COX-2 by activated RAS has been reported in earlier studies (Hoang et al., 2006; Sheng et al., 2001; Sheng et al., 1998), the suppression of HPGD expression represents a previously unrecognized capability of mutant KRAS to inhibit prostaglandin catabolism. Notably, both COX-2 upregulation and HPGD suppression have been reported to cooperate with mutant KRAS and accelerate cancer progression in animal models (Funahashi et al., 2007; Pham et al., 2008). Moreover, in patients with pancreatic or colon adenocarcinoma, a large fraction of which harbor KRAS mutations, high levels of COX-2 and low levels of HPGD correlated with lower overall survival (Figures 6 and S6). Further studies will be required to determine whether the levels of these molecules predict SG upregulation and prognosis. However, given the role of adaptive stress responses in conferring tumorigenic fitness, it is enticing to speculate that the capacity of these molecules to promote the progression of mutant KRAS cancers could be attributed, at least in part, to their essential role in controlling mutant KRAS-dependent upregulation of SGs. It is noteworthy that several epidemiological studies have demonstrated a role for COX inhibitors in the prevention of human cancers (Cooper et al., 2010). It remains to be determined whether, in the context of mutant KRAS tumors, the chemopreventive benefits of COX inhibitors may be related to their ability to impair SG formation *in vivo*.

From a therapeutic perspective, our data indicate that prostaglandins may play a role in the chemoresistance of mutant KRAS cells, in large part due to their capacity to induce the upregulation of SGs. Consequently, targeting the mutant KRAS-driven accumulation of 15-d-PGJ₂, the critical mediator of SG upregulation, is likely to be of therapeutic benefit. In agreement with this postulate, COX-2 inhibition combined with chemotherapy showed a survival advantage in patients with moderate to high levels of COX-2 in a phase II clinical trial (Edelman et al., 2008). Another phase II study in previously untreated COX-2-positive advanced non-small cell lung cancer (NSCLC) patients showed a therapeutic benefit to COX-2 inhibition in combination with platinum-based chemotherapy (Wang et al., 2008). A larger study, however, employing various biomarkers of COX activity and target engagement have reported no meaningful clinical benefit, highlighting the need for more specific strategies for targeting prostaglandin accumulation (Edelman et al., 2015). For example, the development of agents that lower the cellular levels of 15-d-PGJ₂ or specifically inhibit 15-d-PGJ₂ may constitute a useful approach for the chemosensitization of KRAS tumors.

Consistent with the secretory nature of 15-d-PGJ₂, we have found that mutant KRAS can upregulate SGs in a 15-d-PGJ₂-mediated cell non-autonomous fashion. This finding has significant implications, because it is becoming increasingly apparent that cancer cells within a tumor show extensive genetic and phenotypic heterogeneity, thus rendering the design of effective therapies that target all cell populations within tumors a major challenge. The existence of such heterogeneity in tumors harboring mutant KRAS is indicated by reports demonstrating significant variations in KRAS mutational status in lung, colon, and papillary thyroid carcinomas (Baldus et al., 2010; Dieterle et al., 2004; Han et al., 2011; Perez et al., 2013; Richman et al., 2011). Importantly, it has been shown that mutant KRAS clones

can affect the chemosensitivity of non-mutant KRAS clones, rendering them resistant to anti-cancer therapies (Hobor et al., 2014; Molinari et al., 2011). Our results indicate that the cell non-autonomous effect of mutant KRAS cells on SG formation may provide a mechanism for such inter-clonal cooperation. Accordingly, SG upregulation could represent a therapeutic vulnerability that is shared by mutant and WT KRAS tumor cells and, as such, the targeting of this mechanism might represent an effective strategy to eradicate tumor cell communities.

Although the cytoprotective function of SGs is well documented, the precise mechanisms through which SGs confer stress resistance have yet to be established. To date, this capacity has been attributed predominantly to the sequestration of macromolecules—proteins, mRNA, micro RNA (miRNA)—that are linked to regulatory pathways that control cell survival. For example, the recruitment of tumor necrosis factor (TNF) receptor-associated factor (TRAF) to SGs inhibits tumor necrosis factor signaling under stress, thus blocking cellular apoptosis (Kim et al., 2005). Additionally, the global shift in mRNA translation and mRNA stability resulting from the recruitment of mRNA and miRNA to SGs has been postulated to contribute to stress resistance (Kedersha et al., 2013). The macromolecular composition of SGs can vary significantly, depending on the type of stress and the cellular background. In principle, therefore, in a setting of mutant KRAS, SGs may have a distinct composition that, in turn, may impart a unique translational and post-translational stress signature. Clearly, further investigation will be required to understand whether such a signature could be predictive of overall tumor cell resilience and chemotherapeutic resistance.

STAR★METHODS

Detailed methods are provided in the online version of this paper and include the following:

- KEY RESOURCES TABLE
- CONTACT FOR REAGENTS AND RESOURCE SHARING
- EXPERIMENTAL MODEL AND SUBJECT DETAILS
 - Cell lines
 - Mice
 - Human Pancreas Specimens
- METHOD DETAILS
 - Constructs
 - Stress and inhibitor treatments
 - Conditioned media experiments
 - Immunofluorescence and immunohistochemistry
 - Quantification of stress granules
 - Quantitative RT-PCR
 - FACS analysis
 - ELISA
 - Proliferation
 - Analysis of human patient data
- QUANTIFICATION AND STATISTICAL ANALYSIS

SUPPLEMENTAL INFORMATION

Supplemental Information includes six figures and can be found with this article online at <http://dx.doi.org/10.1016/j.cell.2016.11.035>.

AUTHOR CONTRIBUTIONS

E.G. and D.B.-S. conceived the study and co-wrote the manuscript. E.G. conceived and conducted the experiments and data analysis.

ACKNOWLEDGMENTS

We would like to thank Dr. Cristina Hajdu (Department of Pathology, New York University School of Medicine) for providing human pancreatic cancer samples. We are grateful to Dr. Emily Vucic for the genome data analysis of lung and colon adenocarcinoma patients. We thank Dr. Cosimo Commisso and Dr. Yuliya Pulayeva-Gupta for providing tissues samples and technical expertise with animal studies. We thank Dr. Laura Taylor for help with manuscript preparation and the members of the D.B.-S. lab for discussions.

The New York University Langone Medical Center (NYULMC) Office of Collaborative Science Cytometry Core and Histology Core are shared resources partially supported by Cancer Center Support grant P30CA016087 at the Laura and Isaac Perlmutter Cancer Center. This work was supported by NIH grants R01CA055360 (to D.B.-S.) and 1F32CA13922 (to E.G.).

Received: March 14, 2016

Revised: September 23, 2016

Accepted: November 17, 2016

Published: December 15, 2016

REFERENCES

- Abramoff, M.D., Magalhaes, P.J., and Ram, S.J. (2004). Image processing with ImageJ. *Biophoton. Int.* *11*, 36–42.
- Adjibade, P., St-Sauveur, V.G., Quevillon Huberdeau, M., Fournier, M.J., Savard, A., Coudert, L., Khandjian, E.W., and Mazroui, R. (2015). Sorafenib, a multikinase inhibitor, induces formation of stress granules in hepatocarcinoma cells. *Oncotarget* *6*, 43927–43943.
- Aguirre-Gamboa, R., Gomez-Rueda, H., Martínez-Ledesma, E., Martínez-Torteya, A., Chacolla-Huaringa, R., Rodriguez-Barentos, A., Tamez-Peña, J.G., and Treviño, V. (2013). SuryExpress: an online biomarker validation tool and database for cancer gene expression data using survival analysis. *PLoS One* *8*, e74250.
- Anderson, P., Kedersha, N., and Ivanov, P. (2015). Stress granules, P-bodies and cancer. *Biochim. Biophys. Acta* *1849*, 861–870.
- Arimoto, K., Fukuda, H., Imajoh-Ohmi, S., Saito, H., and Takekawa, M. (2008). Formation of stress granules inhibits apoptosis by suppressing stress-responsive MAPK pathways. *Nat. Cell Biol.* *10*, 1324–1332.
- Baldus, S.E., Schaefer, K.L., Engers, R., Hartleb, D., Stoecklein, N.H., and Gabbert, H.E. (2010). Prevalence and heterogeneity of KRAS, BRAF, and PIK3CA mutations in primary colorectal adenocarcinomas and their corresponding metastases. *Clin Cancer Res.* *16*, 790–799.
- Beronja, S., Livshits, G., Williams, S., and Fuchs, E. (2010). Rapid functional dissection of genetic networks via tissue-specific transduction and RNAi in mouse embryos. *Nat. Med.* *16*, 821–827.
- Bordeleau, M.E., Matthews, J., Wojnar, J.M., Lindqvist, L., Novac, O., Jankowsky, E., Sonenberg, N., Northcote, P., Teesdale-Spittle, P., and Pelletier, J. (2005). Stimulation of mammalian translation initiation factor eIF4A activity by a small molecule inhibitor of eukaryotic translation. *Proc. Natl. Acad. Sci. USA* *102*, 10460–10465.
- Brûlet, P., Babinet, C., Kemler, R., and Jacob, F. (1980). Monoclonal antibodies against trophectoderm-specific markers during mouse blastocyst formation. *Proc Natl Acad Sci USA* *7*, 4113–4117.
- Buchan, J.R., and Parker, R. (2009). Eukaryotic stress granules: the ins and outs of translation. *Mol. Cell* *36*, 932–941.
- Campeau, E., Ruhl, V.E., Rodier, F., Smith, C.L., Rahmberg, B.L., Fuss, J.O., Campisi, J., Yaswen, P., Cooper, P.K., and Kaufman, P.D. (2009). A versatile viral system for expression and depletion of proteins in mammalian cells. *PLoS ONE* *4*, e6529.
- Chin, K.V., Ueda, K., Pastan, I., and Gottesman, M.M. (1992). Modulation of activity of the promoter of the human MDR1 gene by Ras and p53. *Science* *255*, 459–462.
- Commisso, C., Davidson, S.M., Soydaner-Azeloglu, R.G., Parker, S.J., Kamphorst, J.J., Hackett, S., Grabocka, E., Nofal, M., Drebin, J.A., Thompson, C.B., et al. (2013). Macropinocytosis of protein is an amino acid supply route in Ras-transformed cells. *Nature* *497*, 633–637.
- Cooper, K., Squires, H., Carroll, C., Papaioannou, D., Booth, A., Logan, R.F., Maguire, C., Hind, D., and Tappenden, P. (2010). Chemoprevention of colorectal cancer: systematic review and economic evaluation. *Health Technol. Assess.* *14*, 1–206.
- Dewey, C.M., Cenik, B., Sephton, C.F., Dries, D.R., Mayer, P., 3rd, Good, S.K., Johnson, B.A., Herz, J., and Yu, G. (2011). TDP-43 is directed to stress granules by sorbitol, a novel physiological osmotic and oxidative stressor. *Mol. Cell. Biol.* *31*, 1098–1108.
- Dieterle, C.P., Conzelmann, M., Linnemann, U., and Berger, M.R. (2004). Detection of isolated tumor cells by polymerase chain reaction-restriction fragment length polymorphism for K-ras mutations in tissue samples of 199 colorectal cancer patients. *Clin Cancer Res.* *10*, 641–650.
- Downward, J. (2015). RAS synthetic lethal screens revisited: still seeking the elusive prize? *Clin Cancer Res.* *21*, 1802–1809.
- Eberhard, D.A., Johnson, B.E., Amler, L.C., Goddard, A.D., Heldens, S.L., Herbst, R.S., Ince, W.L., Jänne, P.A., Januario, T., Johnson, D.H., et al. (2005). Mutations in the epidermal growth factor receptor and in KRAS are predictive and prognostic indicators in patients with non-small-cell lung cancer treated with chemotherapy alone and in combination with erlotinib. *J. Clin. Oncol.* *23*, 5900–5909.
- Edelman, M.J., Watson, D., Wang, X., Morrison, C., Kratzke, R.A., Jewell, S., Hodgson, L., Mauer, A.M., Gajra, A., Masters, G.A., et al. (2008). Eicosanoid modulation in advanced lung cancer: cyclooxygenase-2 expression is a positive predictive factor for celecoxib + chemotherapy—Cancer and Leukemia Group B Trial 30203. *J. Clin. Oncol.* *26*, 848–855.
- Edelman, M.J., Tan, M.T., Fidler, M.J., Sanborn, R.E., Otterson, G., Sequist, L.V., Evans, T.L., Schneider, B.J., Keresztes, R., Rogers, J.S., et al. (2015). Randomized, double-blind, placebo-controlled, multicenter phase II study of the efficacy and safety of apicoxib in combination with either docetaxel or pemetrexed in patients with biomarker-selected non-small-cell lung cancer. *J. Clin. Oncol.* *33*, 189–194.
- Faber, A.C., Coffee, E.M., Costa, C., Dastur, A., Ebi, H., Hata, A.N., Yeo, A.T., Edelman, E.J., Song, Y., Tam, A.T., et al. (2014). mTOR inhibition specifically sensitizes colorectal cancers with KRAS or BRAF mutations to BCL-2/BCL-XL inhibition by suppressing MCL-1. *Cancer Discov.* *4*, 42–52.
- Fournier, M.J., Gareau, C., and Mazroui, R. (2010). The chemotherapeutic agent bortezomib induces the formation of stress granules. *Cancer Cell Int.* *10*, 12.
- Funahashi, H., Satake, M., Dawson, D., Huynh, N.A., Reber, H.A., Hines, O.J., and Eibl, G. (2007). Delayed progression of pancreatic intraepithelial neoplasia in a conditional Kras(G12D) mouse model by a selective cyclooxygenase-2 inhibitor. *Cancer Res.* *67*, 7068–7071.
- Grabocka, E., Pulayeva-Gupta, Y., Jones, M.J., Lubkov, V., Yemanberhan, E., Taylor, L., Jeng, H.H., and Bar-Sagi, D. (2014b). Wild-type H- and N-Ras promote mutant K-Ras-driven tumorigenesis by modulating the DNA damage response. *Cancer Cell* *25*, 243–256.
- Grana, T.M., Rusyn, E.V., Zhou, H., Sartor, C.I., and Cox, A.D. (2002). Ras mediates radioresistance through both phosphatidylinositol 3-kinase-dependent and Raf-dependent but mitogen-activated protein kinase/extracellular signal-regulated kinase kinase-independent signaling pathways. *Cancer Res.* *62*, 4142–4150.
- Han, K., Lee, T.Y., Nikitopoulos, D.E., Soper, S.A., and Murphy, M.C. (2011). A vertically stacked, polymer, microfluidic point mutation analyzer: rapid high accuracy detection of low-abundance K-ras mutations. *Anal. Biochem.* *417*, 211–219.

- Hata, A.N., Yeo, A., Faber, A.C., Lifshits, E., Chen, Z., Cheng, K.A., Walton, Z., Sarosiek, K.A., Letai, A., Heist, R.S., et al. (2014). Failure to induce apoptosis via BCL-2 family proteins underlies lack of efficacy of combined MEK and PI3K inhibitors for KRAS-mutant lung cancers. *Cancer Res.* *74*, 3146–3156.
- Hingorani, S.R., Wang, L., Multani, A.S., Combs, C., Deramaudt, T.B., Hruban, R.H., Rustgi, A.K., Chang, S., and Tuveson, D.A. (2005). Trp53R172H and KrasG12D cooperate to promote chromosomal instability and widely metastatic pancreatic ductal adenocarcinoma in mice. *Cancer Cell* *7*, 469–483.
- Hoang, B., Zhu, L., Shi, Y., Frost, P., Yan, H., Sharma, S., Sharma, S., Goodglick, L., Dubinett, S., and Lichtenstein, A. (2006). Oncogenic RAS mutations in myeloma cells selectively induce cox-2 expression, which participates in enhanced adhesion to fibronectin and chemoresistance. *Blood* *107*, 4484–4490.
- Hobor, S., Van Emburgh, B.O., Crowley, E., Misale, S., Di Nicolantonio, F., and Bardelli, A. (2014). TGF α and amphiregulin paracrine network promotes resistance to EGFR blockade in colorectal cancer cells. *Clin Cancer Res.* *20*, 6429–6438.
- Huss, D., Benazeraf, B., Wallingford, A., Filla, M., Yang, J., Fraser, S.E., and Lansford, R. (2015). A transgenic quail model that enables dynamic imaging of amniote embryogenesis. *Development* *142*, 2850–2859.
- Kaehler, C., Isensee, J., Hucho, T., Lehrach, H., and Krobitsch, S. (2014). 5-Fluorouracil affects assembly of stress granules based on RNA incorporation. *Nucleic Acids Res.* *42*, 6436–6447.
- Kedersha, N., and Anderson, P. (2007). Mammalian stress granules and processing bodies. *Methods Enzymol.* *431*, 61–81.
- Kedersha, N., Tisdale, S., Hickman, T., and Anderson, P. (2008). Real-time and quantitative imaging of mammalian stress granules and processing bodies. *Methods Enzymol.* *448*, 521–552.
- Kedersha, N., Ivanov, P., and Anderson, P. (2013). Stress granules and cell signaling: more than just a passing phase? *Trends Biochem. Sci.* *38*, 494–506.
- Kim, W.J., Back, S.H., Kim, V., Ryu, I., and Jang, S.K. (2005). Sequestration of TRAF2 into stress granules interrupts tumor necrosis factor signaling under stress conditions. *Mol. Cell. Biol.* *25*, 2450–2462.
- Kim, W.J., Kim, J.H., and Jang, S.K. (2007). Anti-inflammatory lipid mediator 15d-PGJ2 inhibits translation through inactivation of eIF4A. *EMBO J.* *26*, 5020–5032.
- Kopetz, S., Desai, J., Chan, E., Hecht, J.R., O'Dwyer, P.J., Maru, D., Morris, V., Janku, F., Dasari, A., Chung, W., et al. (2015). Phase II Pilot Study of Vemurafenib in Patients With Metastatic BRAF-Mutated Colorectal Cancer. *J. Clin. Oncol.* *33*, 4032–4038.
- Luo, J., Emanuele, M.J., Li, D., Creighton, C.J., Schlabach, M.R., Westbrook, T.F., Wong, K.K., and Elledge, S.J. (2009a). A genome-wide RNAi screen identifies multiple synthetic lethal interactions with the Ras oncogene. *Cell* *137*, 835–848.
- Luo, J., Solimini, N.L., and Elledge, S.J. (2009b). Principles of cancer therapy: oncogene and non-oncogene addiction. *Cell* *136*, 823–837.
- McCormick, F. (2015). KRAS as a therapeutic target. *Clin Cancer Res.* *21*, 1797–1801.
- Moeller, B.J., Cao, Y., Li, C.Y., and Dewhirst, M.W. (2004). Radiation activates HIF-1 to regulate vascular radiosensitivity in tumors: role of reoxygenation, free radicals, and stress granules. *Cancer Cell* *5*, 429–441.
- Molinari, F., Felicioni, L., Buscarino, M., De Dosso, S., Buttitta, F., Malatesta, S., Movilia, A., Luoni, M., Boldorini, R., Alabiso, O., et al. (2011). Increased detection sensitivity for KRAS mutations enhances the prediction of anti-EGFR monoclonal antibody resistance in metastatic colorectal cancer. *Clin Cancer Res.* *17*, 4901–4914.
- Nazarian, R., Shi, H., Wang, Q., Kong, X., Koya, R.C., Lee, H., Chen, Z., Lee, M.K., Attar, N., Sazegar, H., et al. (2010). Melanomas acquire resistance to B-RAF(V600E) inhibition by RTK or N-RAS upregulation. *Nature* *468*, 973–977.
- Pazarentzos, E., and Bivona, T.G. (2015). Adaptive stress signaling in targeted cancer therapy resistance. *Oncogene* *34*, 5599–5606.
- Perez, K., Walsh, R., Brilliant, K., Noble, L., Yakirevich, E., Breese, V., Jackson, C., Chatterjee, D., Pricolo, V., Roth, L., et al. (2013). Heterogeneity of colorectal cancer (CRC) in reference to KRAS proto-oncogene utilizing WAVE technology. *Exp. Mol. Pathol.* *95*, 74–82.
- Pham, H., Eibl, G., Vincenti, R., Chong, B., Tai, H.H., and Slice, L.W. (2008). 15-Hydroxyprostaglandin dehydrogenase suppresses K-RasV12-dependent tumor formation in Nu/Nu mice. *Mol. Carcinog.* *47*, 466–477.
- Poulikakos, P.I., Persaud, Y., Janakiraman, M., Kong, X., Ng, C., Moriceau, G., Shi, H., Atefi, M., Titz, B., Gabay, M.T., et al. (2011). RAF inhibitor resistance is mediated by dimerization of aberrantly spliced BRAF(V600E). *Nature* *480*, 387–390.
- Richman, S.D., Chambers, P., Seymour, M.T., Daly, C., Grant, S., Hemmings, G., and Quirke, P. (2011). Intra-tumoral heterogeneity of KRAS and BRAF mutation status in patients with advanced colorectal cancer (aCRC) and cost-effectiveness of multiple sample testing. *Anal. Cell Pathol. (Amst.)* *34*, 61–66.
- Rosell, R., González-Larriba, J.L., Alberola, V., Molina, F., Monzó, M., Benito, D., Pérez, J.M., and de Anta, J.M. (1995). Single-agent paclitaxel by 3-hour infusion in the treatment of non-small cell lung cancer: links between p53 and K-ras gene status and chemosensitivity. *Semin. Oncol.* *22*(6, Suppl 14), 12–18.
- Sheng, H., Williams, C.S., Shao, J., Liang, P., DuBois, R.N., and Beauchamp, R.D. (1998). Induction of cyclooxygenase-2 by activated Ha-ras oncogene in Rat-1 fibroblasts and the role of mitogen-activated protein kinase pathway. *J. Biol. Chem.* *273*, 22120–22127.
- Sheng, H., Shao, J., and Dubois, R.N. (2001). K-Ras-mediated increase in cyclooxygenase 2 mRNA stability involves activation of the protein kinase B1. *Cancer Res.* *61*, 2670–2675.
- Shirasawa, S., Furuse, M., Yokoyama, N., and Sasazuki, T. (1993). Altered growth of human colon cancer cell lines disrupted at activated Ki-ras. *Science* *260*, 85–88.
- Silvera, D., Formenti, S.C., and Schneider, R.J. (2010). Translational control in cancer. *Nat. Rev. Cancer* *10*, 254–266.
- Solimini, N.L., Luo, J., and Elledge, S.J. (2007). Non-oncogene addiction and the stress phenotype of cancer cells. *Cell* *130*, 986–988.
- Stephen, A.G., Esposito, D., Bagni, R.K., and McCormick, F. (2014). Dragging ras back in the ring. *Cancer Cell* *25*, 272–281.
- Wang, L., Chen, W., Xie, X., He, Y., and Bai, X. (2008). Celecoxib inhibits tumor growth and angiogenesis in an orthotopic implantation tumor model of human colon cancer. *Exp. Oncol.* *30*, 42–51.
- Wang, Z., Li, Y., Ahmad, A., Banerjee, S., Azmi, A.S., Kong, D., and Sarkar, F.H. (2011). Pancreatic cancer: understanding and overcoming chemoresistance. *Nat. Rev. Gastroenterol. Hepatol.* *8*, 27–33.
- Wippich, F., Bodenmiller, B., Trajkovska, M.G., Wanka, S., Aebersold, R., and Pelkmans, L. (2013). Dual specificity kinase DYRK3 couples stress granule condensation/dissolution to mTORC1 signaling. *Cell* *152*, 791–805.
- Zhu, J., Sanborn, J.Z., Benz, S., Szeto, C., Hsu, F., Kuhn, R.M., Karolchik, D., Archie, J., Lenburg, M.E., Esserman, L.J., et al. (2009). The UCSC cancer genomics browser. *Nat. Methods* *6*, 239–240.
- Zuber, J., Tchernitsa, O.I., Hinzmann, B., Schmitz, A.C., Grips, M., Hellriegel, M., Sers, C., Rosenthal, A., and Schäfer, R. (2000). A genome-wide survey of RAS transformation targets. *Nat. Genet.* *24*, 144–152.

STAR★METHODS

KEY RESOURCES TABLE

REAGENT or RESOURCE	SOURCE	IDENTIFIER
Antibodies		
Mouse monoclonal G3BP	BD Biosciences	Cat# 611126; clone 23/G3BP; RRID: AB_398437
Mouse monoclonal K-RAS	Santa Cruz Biotechnologies	Cat# sc-30; clone F234; RRID: AB_627865
Mouse monoclonal Erk2	EMD Millipore	Cat# 05-157; clone 1B3B9; RRID: AB_309637
Mouse monoclonal vinculin	Sigma Aldrich	Cat# V9131; clone hVIN-1; RRID: AB_477629
Rabbit polyclonal eIF4G	Santa Cruz Biotechnologies	Cat# sc-11373; clone H-300; RRID: AB_2095750
Rabbit monoclonal phospho-eIF2 α	Cell Signaling	Cat# 3398; clone D9G8; RRID: AB_2096481
Rabbit monoclonal eIF2 α	Cell Signaling	Cat# 5324; clone D7D3; RRID: AB_10692650
Goat polyclonal eIF4A1	Santa Cruz Biotechnologies	Cat# sc-14211; clone N-19; RRID: AB_2097369
Rabbit monoclonal phospho-Erk1/2	Cell Signaling	Cat# 4370; clone D13.14.4E; RRID: AB_2315112
Rabbit monoclonal COX-2	LabVision	Cat# RM9121-S0; clone SP21; RRID: AB_720731
Rabbit polyclonal 15-PGDH	GeneTex	Cat# GTX113465; clone N1C2; RRID: AB_10617920
Rabbit polyclonal 15-deoxy Delta 12,14 Prostaglandin J2 antibody (15-d-PGJ2)	Abcam	Cat#ab2313; RRID: AB_302970
Rat monoclonal CK8	Brület et al., 1980	Developmental Studies Hybridoma Bank Cat#TROMA-I; RRID: AB_531826
Rabbit monoclonal CK19	Abcam	Cat#ab52625; clone EP1580Y; RRID: AB_2281020
Rabbit polyclonal PABP1	Cell Signaling	Cat#4992S; RRID: AB_10693595
Goat anti-Mouse IgG (H+L) Secondary Antibody, Alexa Fluor 488	ThermoFisher	Cat#A-11029; RRID: AB_2534088
Goat anti-Mouse IgG (H+L) Secondary Antibody, Alexa Fluor 555	ThermoFisher	Cat#A-21424; RRID: AB_2535845
Goat anti-Rabbit IgG (H+L) Secondary Antibody, Alexa Fluor 488	ThermoFisher	Cat#A-11034; RRID: AB_2576217
Goat anti-Rabbit IgG (H+L) Secondary Antibody, Alexa Fluor 555	ThermoFisher	Cat#A-21429; RRID: AB_2535850
Goat anti-Rat IgG (H+L) Secondary Antibody, Alexa Fluor 488	ThermoFisher	Cat#A-11006; RRID: AB_2534074
Goat anti-Mouse IgG (H+L) Secondary Antibody, Alexa Fluor 680	ThermoFisher	Cat#A-21058; RRID: AB_2535724
IRDye 800CW Goat anti-Rabbit IgG (H + L)	LI-COR Biosciences	Cat#926-32211; RRID: AB_621843
IRDye 800CW Donkey anti-Goat IgG (H + L)	LI-COR Biosciences	Cat# 925-32214
Chemicals, Peptides, and Recombinant Proteins		
Sodium arsenate	Sigma	Cat#S7400; CAS#7784-46-5
Oxaliplatin	Tocris Bioscience	Cat#2623; CAS#61825-94-3
Velcade (bortezomib)	Santa Cruz Biotechnology	Cat#sc-217785; CAS# 179324-69-7
15-deoxy- $\Delta^{12,14}$ -Prostaglandin J ₂ (15-d-PGJ ₂)	Cayman	Cat#18570; CAS# 87893-55-8
Prostaglandin E2	Tocris Bioscience	Cat#2296; CAS# 363-24-6

(Continued on next page)

Continued

REAGENT or RESOURCE	SOURCE	IDENTIFIER
Diclofenac sodium	Selleck	Cat#S1903; CAS# 15307-79-6
5-[[4-(ethoxycarbonyl)phenyl]azo]-2-hydroxy-benzeneacetic acid	Santa Cruz Biotechnology	Cat#sc-205129; CAS# 78028-01-0
Emetine	Calbiochem	Cat#324693; CAS# 316-42-7
Protein A/G PLUS-Agarose	Santa Cruz Biotechnology	Cat#sc-2003
Prolong Gold Antifade Mountant	Molecular Probes	Cat#P36934
HotStart-IT SYBR Green qPCR Master Mix (2X)	Affymetrix	Cat#75762 500
Puromycin	Calbiochem	Cat# 540411; CAS# 58-58-2
Doxycycline	Sigma	Cat#D9891; CAS# 24390-14-5
Blasticidin	Invitrogen	Cat#R21001; CAS# 3513-03-9
3-[4,5-dimethylthiazol-2-yl]-2,5-diphenyl tetrazolium bromide MTT	Sigma	Cat#M5655; CAS# 298-93-1
Harris hematoxylin	Sigma	Cat#HHS32
Eosin Y aqueous	Sigma	Cat#HT110216
Matrigel	Corning	Cat#CB-40234B
Critical Commercial Assays		
15-deoxy- $\Delta^{12,14}$ -PGJ ₂ ELISA kit	Enzo Lifesciences	Cat#ADI-900-023
Prostaglandin D ₂ -MOX ELISA Kit	Cayman Chemicals	Cat#512011
NucView 405 Caspase-3 substrate	Biotium	Cat#10405
RNeasy Mini Kit	QIAGEN	Cat#74104
QuantiTect Reverse Transcription Kit	QIAGEN	Cat#205311
Experimental Models: Cell Lines		
Human: HT-29	ATCC	Cat#HTB-38; RRID: CVCL_0320
Human: NCI-H747	ATCC	Cat#CCL-252; RRID: CVCL_1587
Human: NCI-H508	ATCC	Cat#CCL-253; RRID: CVCL_1564
Human: SNU-C1	ATCC	Cat#CRL-5972; RRID: CVCL_1708
Human: MIA PaCa-2	ATCC	Cat#CRL-1420; RRID: CVCL_0428
Human: PANC-1	ATCC	Cat#CRL-1469; RRID: CVCL_0480
Human: AsPC-1	ATCC	Cat#CRL-1682; RRID: CVCL_0152
Human: Capan-2	ATCC	Cat#HTB-80; RRID: CVCL_0026
Human: Hs 700T	ATCC	Cat#HTB-147; RRID: CVCL_0858
Human: DLD-1	Laboratory of Mark Philips (Luo et al., 2009a; Shirasawa et al., 1993)	Cat# NA
Human: DLD-1 K-RAS ^{WT/-}	Laboratory of Mark Philips (Luo et al., 2009a; Shirasawa et al., 1993)	Cat# NA
Human: HeLa	ATCC	Cat#CCL2; RRID: CVCL_0030
Experimental Models: Organisms/Strains		
Mouse: NCr-Foxn1 ^{nu}	Taconic	Cat#NCRNU; RRID: IMSR_TAC:ncnu
Mouse: LSL-Kras ^{G12D/+} ; LSL-Trp53 ^{R172H/+} ; Pdx-1-Cre	Hingorani et al., 2005	Cat#NA
Recombinant DNA		
pLenti CMV/TO GFP-Zeo DEST (719-1)	Campeau et al., 2009	Addgene Cat#17431
pLenti CMV TetR Blast (716-1)	Campeau et al., 2009	Addgene Cat#17492
pLenti.PGK.H2B-chFP.W	Huss et al., 2015	Addgene Cat#51007
LV-GFP	Beronja et al., 2010	Addgene Cat#25999
Sequence-Based Reagents		
Kras shRNA V2THS-275818	Open Biosystems	V2THS-275818

(Continued on next page)

Continued

REAGENT or RESOURCE	SOURCE	IDENTIFIER
Primer: <i>GAPDH</i> forward AAGGTGAAGGTCGGAGTCAA	This paper	N/A
Primer: <i>GAPDH</i> reverse AATGAAGGGGTCATTGATGG	This paper	N/A
Primer: <i>COX2</i> forward GGCTCAAACATGATGTTTGCA	This paper	N/A
Primer: <i>COX2</i> reverse CCTCGCTTATGATCTGTCTTGA	This paper	N/A
Primer: <i>HPGD</i> forward GAAGGCGGCATCATTATCAA	This paper	N/A
Primer: <i>HPGD</i> reverse GCCATGCTTTGAAGCACAA	This paper	N/A
Software and Algorithms		
ImageJ	Abramoff et al., 2004	https://imagej.nih.gov/ij RRID:SCR_003070
UCSC Cancer Browser	Zhu et al., 2009	https://genome-cancer.ucsc.edu/ ; RRID:SCR_011796
SurvExpress	Aguirre-Gamboa et al., 2013	http://bioinformatica.mty.itesm.mx:8080/Biomatec/SurvivaX.jsp
SoftWoRx version 6.5.2		http://www.gelifesciences.com/webapp/wcs/stores/servlet/productById/en/GELifeSciences/29065728
Graphpad Prism 7		http://www.graphpad.com/scientific-software/prism/

CONTACT FOR REAGENTS AND RESOURCE SHARING

As Lead Contact, Dafna Bar-Sagi is responsible for all reagent and resource requests. Please contact Dafna Bar-Sagi at dafna.bar-sagi@nyumc.org with requests and inquiries.

EXPERIMENTAL MODEL AND SUBJECT DETAILS**Cell lines**

Human colon cancer cell lines DLD1, HT-29, NCI-H747, NCI-H508, SNUC-1, human pancreatic cancer cell lines Mia-PaCa-2, Panc-1, AsPC1, Capan2, Hs700T, and HEK293T cells and HeLa cells and were obtained from and cultured as indicated by American Type Culture Collection. The isogenic colon cancer cells DLD-1 K-RAS^{WT/G12D} (DLD1 Mut) and DLD1 K-RAS^{WT/-} (DLD1 KO; where the *K-RasG12D* allele has been knocked out by homologous recombination) ([Luo et al., 2009a](#); [Shirasawa et al., 1993](#)) were a kind gift from Dr. Mark Philips. DLD1 Mut and DLD1 KO cells were cultured in RPMI medium with 10% fetal bovine serum and 1% penicillin/streptomycin.

To generate HeLa Tet-ON KRASV12 (HTO-KRASV12), following viral particle production and transduction (MOI = 1), HeLa cells that had efficiently integrated the pLenti CMV/TO KRASV12 construct were obtained by fluorescent sorting based on the GFP marker. Sorted cells were subsequently transduced with a pLenti-CMV TetR Blast (Addgene) and selected with blasticidin (7 μ g/ml). pLenti CMV TetR Blast (716-1) was a gift from Dr. Eric Campeau (Addgene plasmid #17492) ([Campeau et al., 2009](#)). All expression experiments were performed on day 2 of doxycycline (1 μ g/ml) induction.

To generate mCherry-H2B NCI-H508 cells and GFP-H2B DLD1 Mut cells, NCI-H508 and DLD1 Mut cells were transduced with a pLenti.PGK.H2B-chFP.W and LV-GFP respectively. pLenti.PGK.H2B-chFP.W was a gift from Dr. Rusty Lansford (Addgene plasmid # 51007) ([Huss et al., 2015](#)). LV-GFP was a gift from Dr. Elaine Fuchs (Addgene plasmid # 25999) ([Beronja et al., 2010](#)).

To generate PL45, Panc-1, Mia-PaCa-2, and AsPC-1 cells inducibly expressing scramble shRNA or KRAS shRNA, cells were transduced with lentiviral particles [multiplicity of infection (MOI) 7] containing pTripz scramble shRNA or KRAS shRNA (Open Biosystems) and selected with puromycin for 3 days. All knockdown experiments were performed on day 4 of doxycycline (1 μ g/ml) induction.

Mice

For xenografts, female homozygous NCr nude mice (Taconic) were injected subcutaneously in both flanks at 8 weeks of age with 1×10^6 indicated cells mixed at a 1:1 dilution with BD Matrigel (BD Biosciences) in a total volume of 100 μ L. When tumors reached an

average volume of $\sim 500 \text{ mm}^3$ they were excised rapidly, fixed in formalin, and embedded in paraffin as previously described (Grabocka et al., 2014b). For the autochthonous model, pancreata from *LSL-KRas^{G12D};p53^{R172H/+};pdx-Cre* (KPC) mice at 17 weeks of age or control wild-type littermates were isolated and embedded in paraffin. All animal work was approved by New York University Langone Medical Center Institutional Animal Care and Use Committee.

Human Pancreas Specimens

The use of human tissue was reviewed and approved by the Institutional Review Board of NYU School of Medicine and samples (provided by the Tissue Acquisition and Biorepository Service) were obtained after informed consent. Sections (5 μm) were cut from formalin-fixed paraffin-embedded samples for the purpose of immunostaining. A total of 6 pancreatic adenocarcinoma and 3 normal tissues adjacent to PDACs were analyzed.

METHOD DETAILS

Constructs

To generate pLenti-CMV/TO GFP KRASV12 the coding sequence for KRASV12 was cloned into the pLenti-CMV/TO GFP-Zeo Destination vector. pLenti CMV/TO GFP-ZEO Dest (719-1) was a gift from Dr. Eric Campeau (Addgene plasmid # 17431) (Campeau et al., 2009). The constructs encoding mCherry-KRASV12, mCherry-KRASV12T35S, mCherry-KRASV12E37G, and mCherry-KRASV12Y40C were generated by cloning the corresponding KRAS mutants into the mCherry-C1 vector.

Stress and inhibitor treatments

Sodium arsenate was dissolved in dH_2O as a 100mM solution. Oxaliplatin was dissolved in DMSO as 100 mM solutions. Velcade was dissolved in DMSO as a 1 mM solution. UV-C irradiation was performed with Stratalinker 2400 (Agilent Technologies). Stress treatments were performed when cells had reached $\sim 80\%$ confluency. Before treatment cells were serum starved overnight. Stress treatments were performed by treating the cells with vehicle alone or with the different stress inducers: sodium arsenate (100 μM), UV-C (50 mJ/m^2), oxaliplatin (100 μM), velcade (1 μM) for the indicated time points. For 15-d-PGJ2 treatments, cells were treated with 50 μM 15-d-PGJ2 (50mM stock solution in dH_2O) for 1 hr. For COX-1/2 inhibition, cells were treated with 20 μM diclofenac sodium (50 mM stock solution in dH_2O) for 16 hr. For HPGD inhibition, cells were treated with 20 μM 5-[[4-(ethoxycarbonyl)phenyl]azo]-2-hydroxy-benzeneacetic acid (20mM stock solution in DMSO) for 6 hr. For emetine inhibition of stress granules, cells were treated with 40 $\mu\text{g}/\text{ml}$ emetine (40 mg/ml stock solution in dH_2O).

Conditioned media experiments

To prepare conditioned medium, DLD1 Mut and DLD1 KO cells were grown to 70% confluency, washed three times with serum-free medium, and then incubated in serum-free medium for 20 hr. The medium from each cell type was harvested, centrifuged to eliminate intact cells, and supernatant was mixed 1:1 with serum free medium. For control treatments DLD1 Mut and DLD1 KO cells were incubated with conditioned media from DLD1 Mut and DLD1 KO cells, respectively, 10 min prior to stress treatment and medium was not changed for the remainder of the treatment. For KCM treatment DLD1 KO cells were incubated with conditioned media from DLD1 Mut as described above 10 min prior to stress treatment and medium was not changed for the remainder of the treatment. For immunodepletion experiments, KCM was incubated with anti-IgG (3 μg) or anti-15-d-PGJ2 (3 μg) for 3 hr at 4°C . Subsequently, 50 μL of prewashed protein A/G Sepharose resin was added to the mix and incubated at 4°C for 2 hr. Immunodepleted supernatants were separated from protein A/G Sepharose beads by centrifugation. Immunodepleted supernatants were each mixed 1:1 with serum free medium and added to cells 10 min prior to stress treatment.

Immunofluorescence and immunohistochemistry

Cells were grown on coverslips, fixed, and immunostained with antibodies for the established stress granule markers G3BP and eIF4G, as previously described (Kedersha and Anderson, 2007). For assessing stress granules in tissue samples, 5 μm thick paraffin sections were immunostained with anti-G3BP utilizing previously established procedures (Grabocka et al., 2014b). Slides were mounted in ProlongGold (Invitrogen). Imaging was performed using a DeltaVision Elite inverted microscope system (Applied Precision), using a 60 \times /1.4NA Oil PSF Objective from Olympus. The system was equipped with a CoolSNAP HQ2 camera and SoftWoRx imaging software version 5.0. 25 serial optical sections were captured every 0.2- μm and processed using the SoftWoRx deconvolution algorithm and projected into one maximum intensity projection picture using SoftWoRx software (Applied Precision). Images from each dataset were acquired on the same day using the same exposure times. For histology, deparaffinized sections (5 μm) were stained with Harris hematoxylin and eosin according to previously reported procedures (Grabocka et al., 2014b). Images were obtained using a Nikon Eclipse 80i microscope.

Quantification of stress granules

Stress granules were quantified using ImageJ (<https://imagej.nih.gov/ij/>) as previously described (Commisso et al., 2013). Briefly, images were randomly acquired in 4 different fields with at least 50 cells/field. Background intensity was subtracted from each image.

The plug in “Analyze Particles” was used to measure the total area of stress granules/total cell area, average size of SGs, and number of SGs/cell. The total cell area/image was delineated and measured through ImageJ selection and measure area tools. The stress granule index was determined by computing the total stress granule area in relation to the total cell area for each field, and then averaged across all fields.

Quantitative RT-PCR

The RNeasy mini kit (QIAGEN) and QuantiTect reverse transcription kit (QIAGEN) were respectively used for the extraction and reverse transcription of total RNA from cells. SYBR Green PCR Master Mix (USB) was used for amplification and the samples were run on the Stratagene Mx 3005P. The standard curve method was used to quantify gene expression. Expression was normalized to GAPDH.

FACS analysis

Staining for cleaved caspase 3 positive cells was performed using the Nucview-405 Caspase 3 Kit (Biotium) according to the manufacturer’s protocol. Flow cytometry was performed on an LSRII (BD Biosciences) instrument at NYU School of Medicine Flow Cytometry Core Facility, and data were analyzed using FlowJo software.

ELISA

15-d-PGJ2 and PGD2 levels in conditioned medium were measured by Elisa kits (15-d-PGJ2 from Enzo Lifesciences and PGD2-MOX from Cayman Chemicals) following the manufacturer’s instructions.

Proliferation

For viability assays, cells were seeded at a density of 4000 cells/well in 96 well plates. Twenty-four hr post plating, cells were incubated in DMEM with 0.5% serum overnight and subsequently treated with oxaliplatin for 48 hr. Cell viability was assessed by the MTT (3-[4,5-dimethylthiazol-2-yl]-2,5-diphenyl tetrazolium bromide; Sigma-Aldrich) assay according to the manufacturer’s protocol. Viable fraction is expressed as the percentage of vehicle treated control cells.

Analysis of human patient data

We analyzed the publicly available datasets of the UCSC Cancer Browser (<https://genome-cancer.ucsc.edu>). To retrace the exact Kaplan–Meyer analysis for the analysis of PDA patients stratified by PTGS2/HPGD, please visit SurvExpress <http://bioinformatica.mty.itesm.mx:8080/Biomatec/SurvivaX.jsp> (Aguirre–Gamboa et al., 2013).

QUANTIFICATION AND STATISTICAL ANALYSIS

Data were analyzed by the Graphpad Prism built-in test (unpaired, two-tailed), and results were considered significant at $p < 0.05$. Statistical parameters including number of replicates, fold-change or log fold-change, SEM, SD, and statistical significance are reported in the figures and supplemental data.

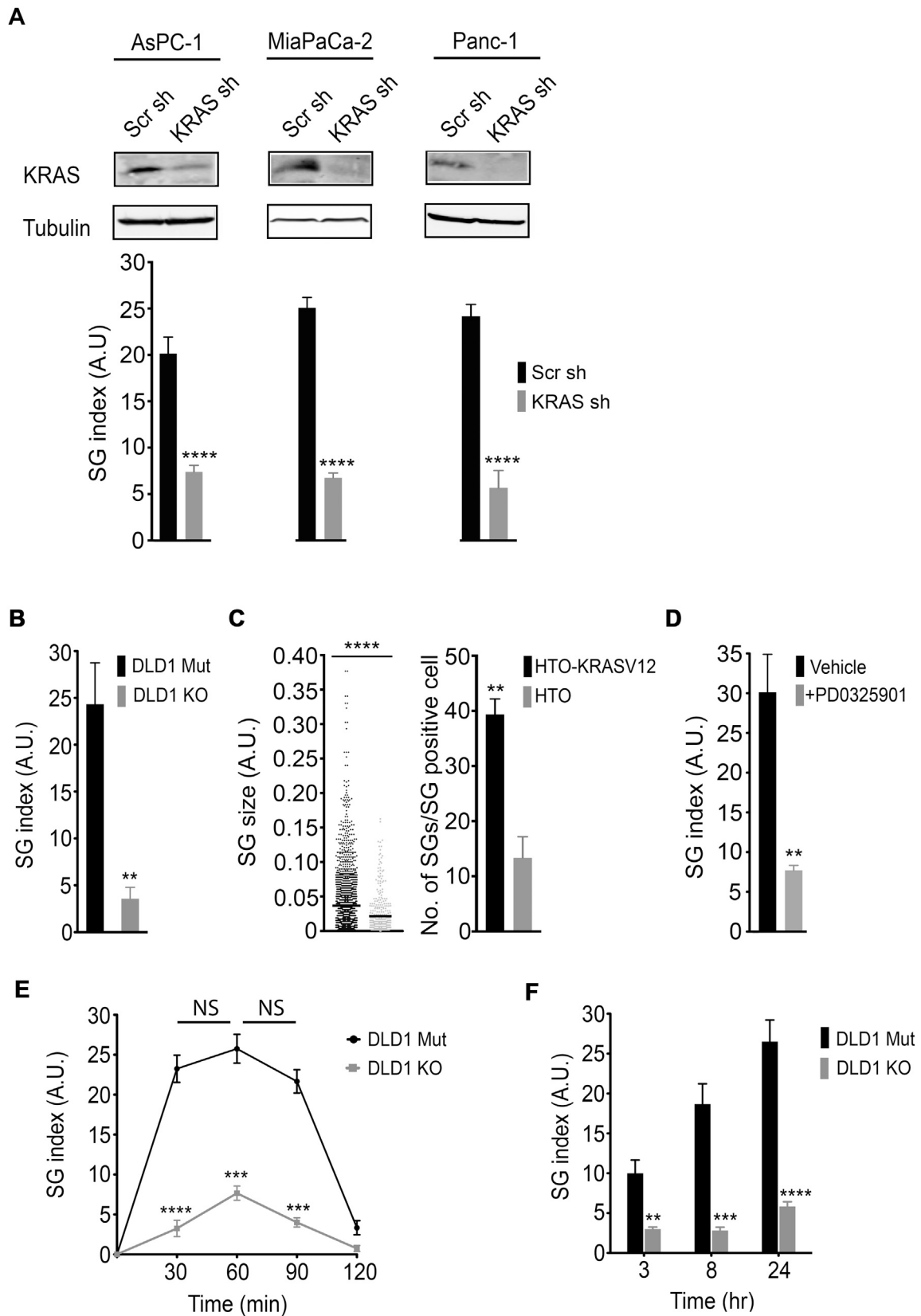


Figure S1. Mutant KRAS Is Necessary and Sufficient for SG Upregulation, Related to Figure 1

(A) *Top*-Whole cell lysates (WCL) from AsPC1, MiaPaCa-2, and Panc-1 cells expressing inducible scramble (Scr) or KRAS shRNA were subjected to immunoblotting with the indicated antibodies. Tubulin serves as a loading control. Blots are representative of at least 3 independent experiments. *Bottom*-AsPC-1, MiaPaCa-2, and Panc-1 cells expressing inducible scramble (Scr) or KRAS shRNA were treated with SA. SG index based on G3BP immunofluorescence is shown.

(B) SG index in DLD1 Mut and DLD1 KO cells treated with SA (100 μ M, 1hr). based on eIF4G immunofluorescence.

(C) HeLa Tet-ON cells (HTO) and HTO cells that conditionally express mutant KRAS (HTO-KRASV12) were treated with SA (100 μ M, 30 min). SG size distribution (left, each dot represents one SG; ●, HTO-KRASV12, ●, HTO) and average number of SGs/SG-positive cell (right) were determined based on G3BP immunofluorescence.

(D) HTO-KRASV12 treated +/- PD0325901 (1 μ M, 20 hr) were subjected to SA (100 μ M, 1hr). SG index was determined based on G3BP immunofluorescence.

(E and F) DLD1 Mut and DLD1 KO cells were treated with 100 μ M sodium arsenate (E) or UV-C (50 mJ/m²) (F). SG index was determined at the indicated time points based on G3BP immunofluorescence.

Data are from a representative experiment out of at least 3 independent experiments. Error bars indicate mean +/- SEM for at least 4 fields of view with at least 50 cells/field of view. **p < 0.01, ***p < 0.001, ****p < 0.0001.

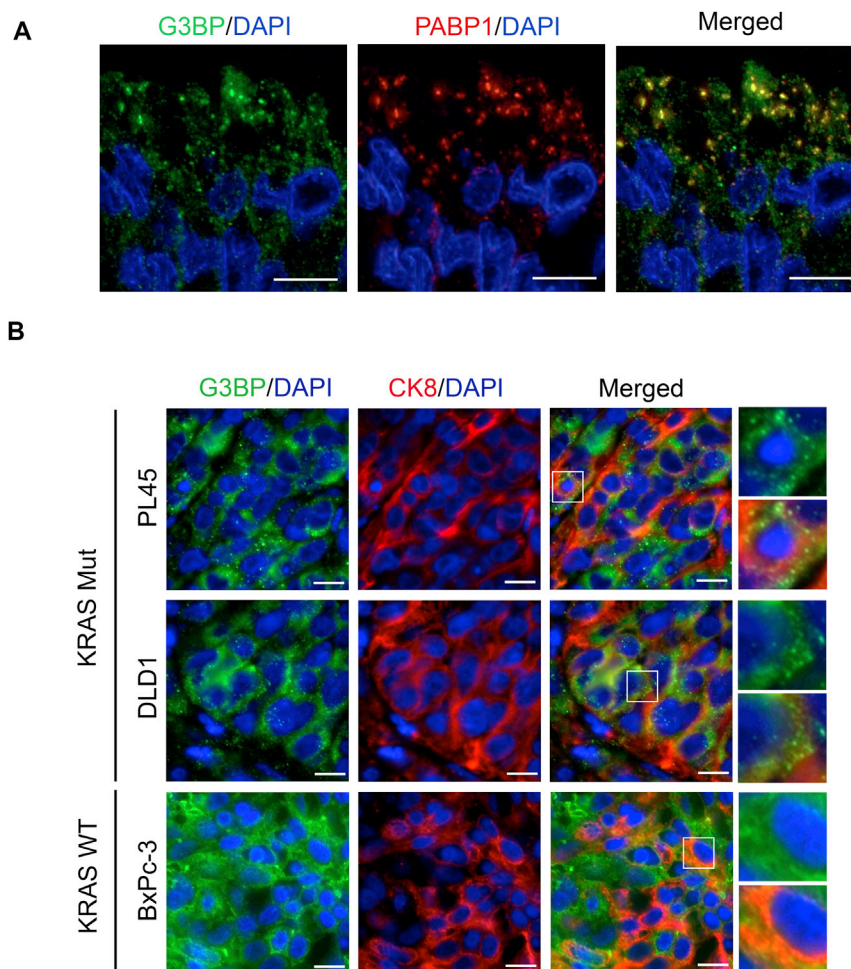


Figure S2. Mutant KRAS Upregulates SGs In Vivo, Related to Figure 2

(A) Sections from two independent human PDAC tissues were immunostained for G3BP and PABP1.

(B) Sections from subcutaneous xenograft tumors of KRAS Mut (PL45, DLD1) and KRAS WT (BxPC-3) cells were immunostained for G3BP and CK8 (epithelial marker). Scale bar 10 μm. Images are representative from 3 animals per cohort. High magnification of boxed areas (3x zoom-in) are shown on the right.

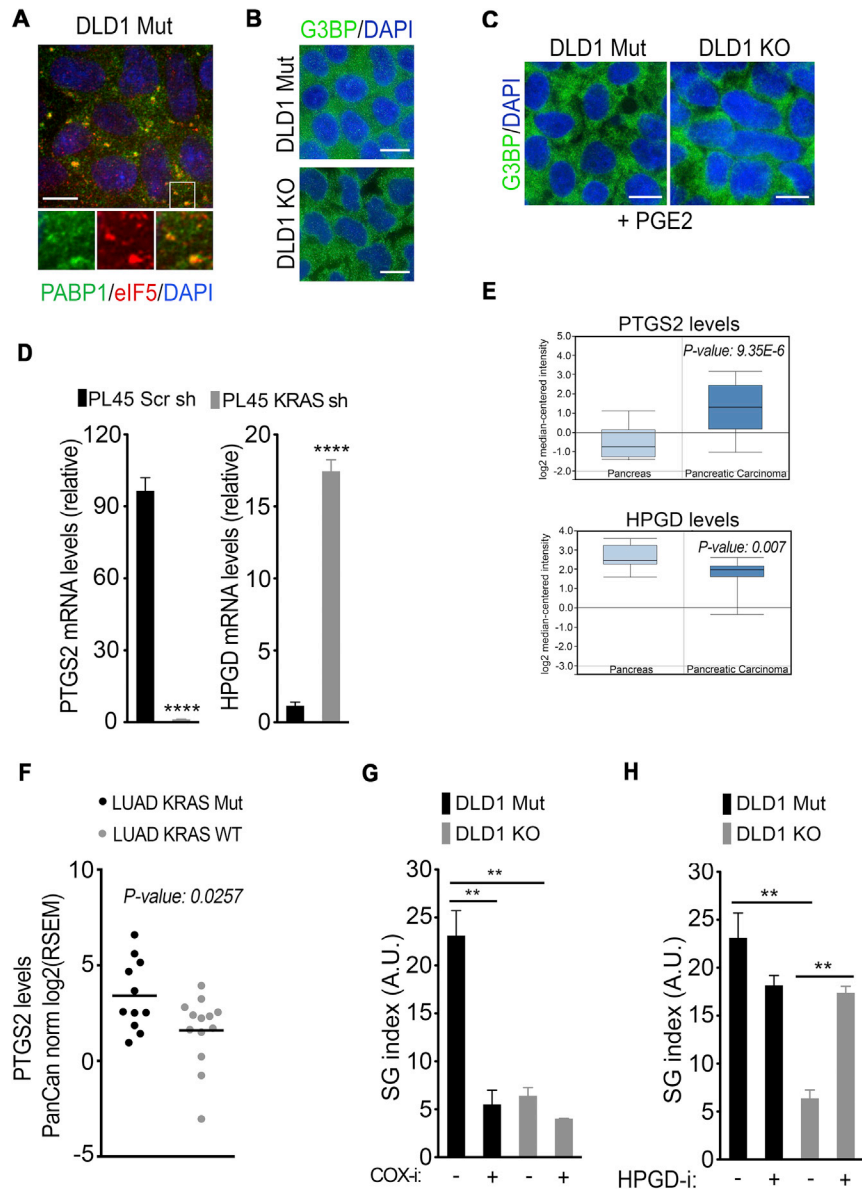


Figure S3. Mutant KRAS Upregulates Prostaglandin Biosynthesis to Promote SG Formation, Related to Figure 3

(A) DLD1 Mut cells were treated with SA as in Figure 3A and SGs were detected by immunofluorescence staining for PABP1 and eIF5.

(B) Untreated DLD1 Mut and DLD1 KO cells were immunostained for G3BP (control corresponding to Figure 3C).

(C) DLD1 Mut and DLD1 KO cells were treated with PGE2 (50 μ M, 1hr) and immunostained for G3BP.

(D) COX-2 and HPGD mRNA levels in PL45 cells expressing scramble (Scr) and KRAS shRNA were assessed by quantitative RT-PCR. Error bars indicate SEM (n = 3).

(E) Levels of COX-2 in Pei pancreatic carcinoma (top) cohorts and the levels of HPGD in Ishikawa pancreatic carcinoma (bottom) cohorts versus normal pancreas. (Oncomine). Error bars indicate SD.

(F) Level 3 Pan-cancer normalized Illumina HiSeq V2 TCGA LUAD mRNA data and corresponding clinical data were downloaded from the UCSC Cancer Browser (<https://genome-cancer.ucsc.edu>). Samples were filtered for those fulfilling the following criteria: primary tumor, KRAS mutational profiling results, tobacco smoking history known, Current smoker and Current reformed smoker for < or = 15 years, for a total of 24 tumors (n = 11 KRAS Mut, n = 13 KRAS WT). The lines indicate the mean.

(G) DLD1 Mut cells were treated as in Figure 3F. SG index based on eIF4G immunofluorescence is shown.

(H) DLD1 Mut and DLD1 KO cells were treated as in Figure 3H. SG index based on eIF4G immunofluorescence is shown.

(C, G–H) Data are from a representative experiment out of at least 3 independent experiments. Error bars indicate mean \pm SEM for at least 4 fields of view with at least 50 cells/field of view. **p < 0.05, ****p < 0.0005.

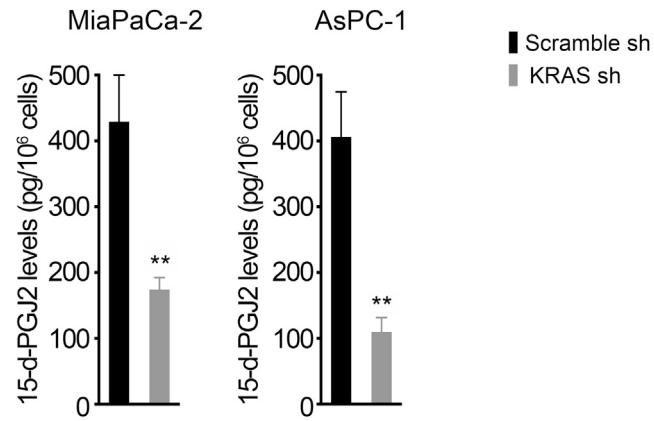


Figure S4. KRAS Knockdown Impairs Secreted 15-d-PGJ2 Levels, Related to Figure 4

The levels of 15-d-PGJ2 that were secreted by MiaPaCa-2 and AsPC-1 cells expressing inducible scramble (Scr) or KRAS shRNA were determined by ELISA of the respective cell culture medium. Data are represented as mean \pm SEM. ** $p < 0.05$.

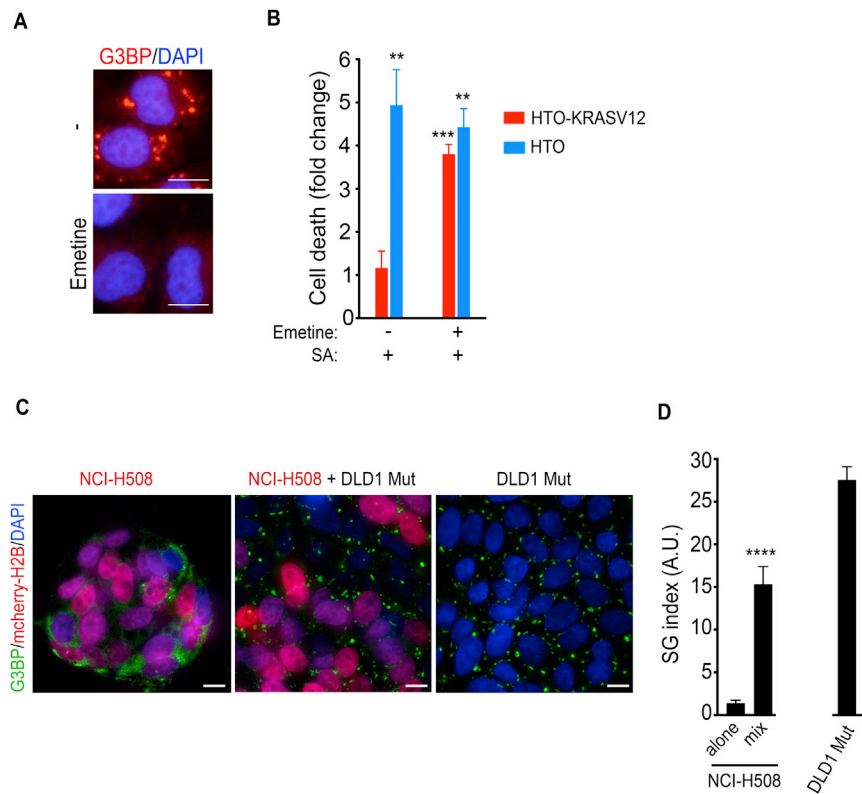


Figure S5. Upregulation of SGs Protects KRAS Mutant Cells from Apoptosis, Related to Figure 5

(A and B) HTO-KRASV12 and HTO cells were treated with SA (100 μ M, 1 hr) in the presence or absence of emetine (40 μ g/ml). (A) SGs were detected by G3BP immunofluorescence staining. (B) Cell death was assessed by analysis of NucView Alexa 405 positive cells from least 4 fields of view with at least 50 cells/field of view. Scale bar 10 μ m. Error bars indicate SEM (n = 3). **p < 0.05, ***p < 0.005.

(C) mCherry-H2B-labeled NCI-H508 cells cultured alone or co-cultured with DLD1 Mut cells were treated with oxaliplatin as in Figures 5D-5E. SGs were detected by G3BP immunofluorescence staining. Scale bar 10 μ m.

(D) SG index in NCI-H508 cells cultured alone, NCI-H508 cells co-cultured with DLD1 Mut cells, and DLD1 Mut cells alone treated as in A. SG index based on G3BP immunofluorescence is shown. Data are from a representative experiment out of least 3 independent experiments. Error bars indicate mean \pm SEM for at least 4 fields of view with at least 50 cells/field of view. ****p < 0.0001.

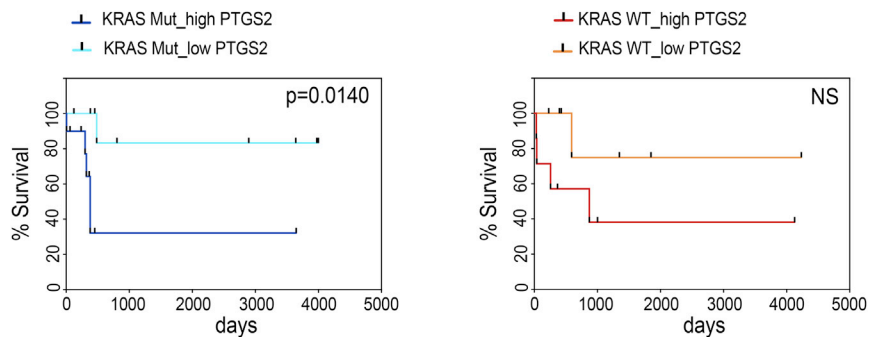


Figure S6. High PTGS2 Expression Correlates with Poorer Recurrence-free Survival in Colon Adenocarcinoma Patients with KRAS-Mutated Tumors, but Not in Patients with WT KRAS, Related to Figure 6

Level 3 Pan-cancer normalized Illumina HiSeq V2 COAD mRNA data and corresponding clinical data were downloaded from the UCSC Cancer Browser (<https://genome-cancer.ucsc.edu>). Samples were filtered for those fulfilling the following criteria: primary tumor and KRAS mutational profiling results, for a total of 48 tumors (n = 23 KRAS Mut, n = 25 KRAS WT). Patients in each cohort (ie. KRAS Mut and WT) were then stratified by PTGS2 tumor expression, into high (top third) and low (bottom third) expression cohorts. Recurrence free survival was plotted using the Kaplan-Meier method and survival curves were compared by Log-rank (Mantel-Cox) tests.